iScience

CellPress
OPEN ACCESS

Article

Epigenetic Regulation of Wnt Signaling by Carboxamide-Substituted Benzhydryl Amines that Function as Histone Demethylase Inhibitors

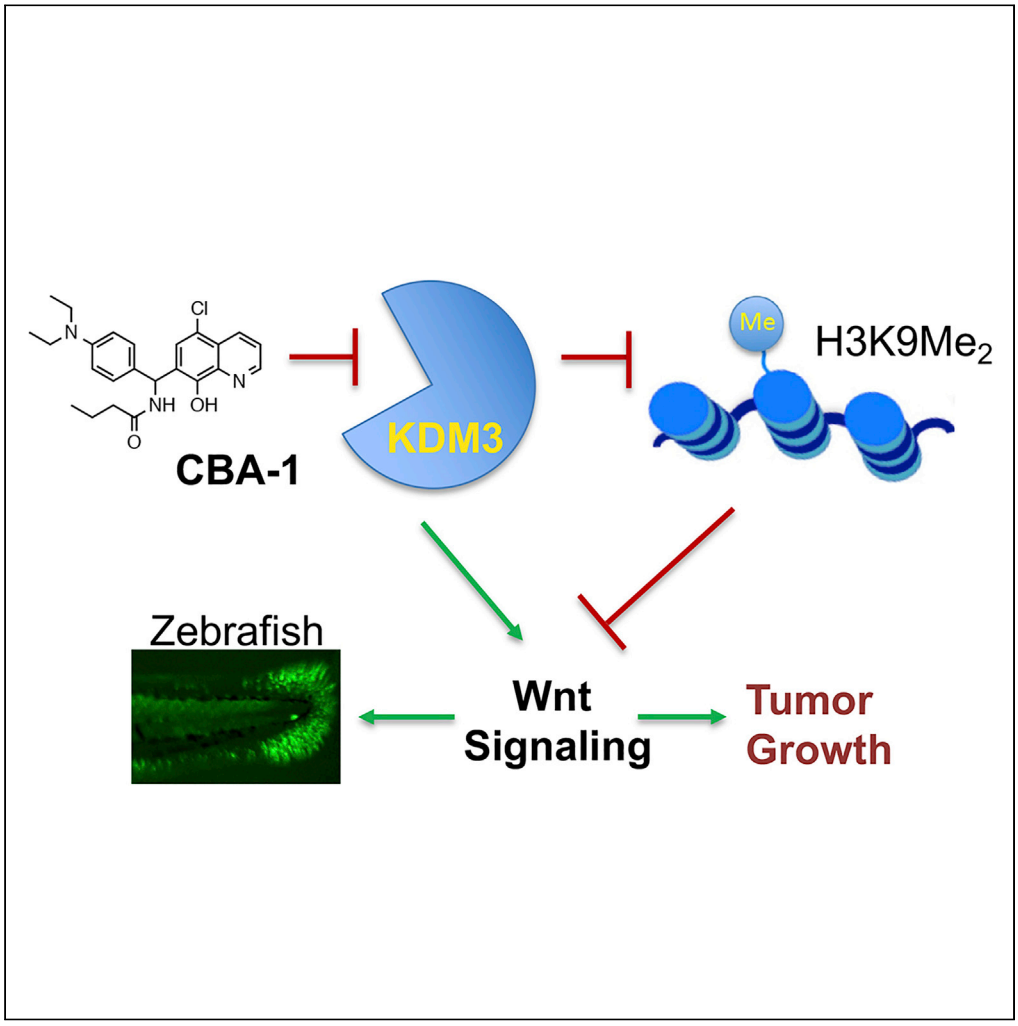

Wen Zhang, Vitaliy M. Sviripa, Yanqi Xie, ..., Chang-Guo Zhan, David S. Watt, Chunming Liu

dwatt@uky.edu (D.S.W.)
chunming.liu@uky.edu (C.L.)

HIGHLIGHTS

A class of carboxamide-substituted benzhydryl amine (CBA) Wnt inhibitors

A biological active, biotinylated CBA to identify KDM3A as a direct target

CBA-1 interacted with the Mn^{2+} ion in the JmjC domains of KDM3A/3B

CBA-1 inhibited Wnt signaling in colon cancer cells and in zebrafish models

Zhang et al., iScience *23*, 101795
December 18, 2020
https://doi.org/10.1016/j.isci.2020.101795

iScience

CellPress
OPEN ACCESS

Article

Epigenetic Regulation of Wnt Signaling by Carboxamide-Substituted Benzhydryl Amines that Function as Histone Demethylase Inhibitors

Wen Zhang,[1,2,6] Vitaliy M. Sviripa,[2,3,4,6] Yanqi Xie,[1,2] Tianxin Yu,[1,2] Meghan G. Haney,[1,2] Jessica S. Blackburn,[1,2] Charles A. Adeniran,[4,5] Chang-Guo Zhan,[3,4,5] David S. Watt,[1,2,3,*] and Chunming Liu[1,2,7,*]

SUMMARY

Aberrant activation of Wnt signaling triggered by mutations in either *Adenomatous Polyposis Coli* (*APC*) or *CTNNB1* (β-catenin) is a hallmark of colorectal cancers (CRC). As part of a program to develop epigenetic regulators for cancer therapy, we developed carboxamide-substituted benzhydryl amines (CBAs) bearing either aryl or heteroaryl groups that selectively targeted histone lysine demethylases (KDMs) and functioned as inhibitors of the Wnt pathway. A biotinylated variant of *N*-((5-chloro-8-hydroxyquinolin-7-yl) (4-(diethylamino)phenyl)-methyl) butyramide (CBA-1) identified KDM3A as a binding partner. KDM3A is a Jumonji (JmjC) domain-containing demethylase that is significantly upregulated in CRC. KDM3A regulates the demethylation of histone H3's lysine 9 ($H3K9Me_2$), a repressive marker for transcription. Inhibiting KDM3 increased $H3K9Me_2$ levels, repressed Wnt target genes, and curtailed *in vitro* CRC cell proliferation. CBA-1 also exhibited *in vivo* inhibition of Wnt signaling in a zebrafish model without displaying *in vivo* toxicity.

INTRODUCTION

Colorectal cancer (CRC) is an unrelenting cause of worldwide, cancer-related mortality with unfortunately high levels in the United States. Many colorectal cancers involve dysfunctional protein participants in the Wnt signaling pathway driven by mutations in either the *Adenomatous Polyposis Coli* (*APC*) gene or the *CTNNB1* (β-catenin) gene (Anastas and Moon, 2013; Kinzler and Vogelstein, 1996; Nusse and Clevers, 2017; Zhong and Virshup, 2020). In normal cells, β-catenin undergoes phosphorylation by casein kinase-1α (CK1α) and glycogen synthase kinase-3 (GSK3) and the phosphorylated β-catenin subsequently recruits multiprotein Skp1-Cullin-F-box (SCF) Ring-type E3 ligase (β-TrCP) that promotes the ubiquitination of β-catenin and initiates its proteasomal degradation (Anastas and Moon, 2013; Nusse and Clevers, 2017). In CRC cells, the APC and β-catenin mutations not only prevent this normal β-catenin phosphorylation and ubiquitination but also promote abnormal β-catenin stabilization, translocation, and nuclear accumulation (Liu et al., 1999, 2002; Yang et al., 2006). In the nucleus, β-catenin binds T cell factor/lymphoid enhancer-binding factor (TCF/LEF) and its co-activators, such as CBP/p300 and Bcl9, and activates the transcription of Wnt target genes, including many oncogenes (Anastas and Moon, 2013; Nusse and Clevers, 2017). The crucial role played by Wnt signaling in CRC progression makes it a challenging but viable target for the development of new antineoplastic agents (Anastas and Moon, 2013; Barker and Clevers, 2006; Garber, 2009; Zhong and Virshup, 2020).

Many reported inhibitors target upstream events in the Wnt signaling pathway and induce β-catenin degradation (Chen et al., 2009; Huang et al., 2009; Liu et al., 2013). For example, a tankyrase inhibitor, XAV939, stabilizes Axin and induces β-catenin degradation (Huang et al., 2009). Porcupine (PORCN) inhibitors, IWP2 and LSK-974, inhibit Wnt processing and secretion. Although these inhibitors affect Wnt signaling in normal cells or cancer cells with wild-type APC, Axin, and β-catenin, they are less effective for many CRC cells containing Wnt pathway mutations than for those cancer cells lacking these mutations. To address this problem, we seek to develop Wnt inhibitors targeting key steps that lie downstream of β-catenin, such as β-catenin nuclear translocation and β-catenin-mediated gene expression (Lyou et al., 2017), or to develop inhibitors of mitochondrial oxidative phosphorylation that also repress Wnt signaling (Zhang et al., 2019). Others, who also recognized this need, seek to develop Wnt inhibitors that alter the

[1]Department of Molecular and Cellular Biochemistry, College of Medicine, University of Kentucky, Lexington, KY 40536-0509, USA

[2]Lucille Parker Markey Cancer Center, University of Kentucky, Lexington, KY 40536-0093, USA

[3]Center for Pharmaceutical Research and Innovation, College of Pharmacy, University of Kentucky, Lexington, KY 40536-0596, USA

[4]Department of Pharmaceutical Sciences, College of Pharmacy, University of Kentucky, Lexington, KY 40536-0596, USA

[5]Molecular Modeling and Pharmaceutical Center, College of Pharmacy, University of Kentucky, Lexington, KY 40536-0596, USA

[6]These authors contributed equally

[7]Lead Contact

*Correspondence: dwatt@uky.edu (D.S.W.), chunming.liu@uky.edu (C.L.)

https://doi.org/10.1016/j.isci.2020.101795

β-catenin/TCF interaction (Lee et al., 2013; Lepourcelet et al., 2004; Schneider et al., 2018), the β-catenin-Bcl9 interactions (Feng et al., 2019; Wisniewski et al., 2016), or the β-catenin/CBP interaction (Emami et al., 2004; Lenz and Kahn, 2014).

Histone methylation events on various lysine residues either activate or repress transcription (Greer and Shi, 2012; Hyun et al., 2017). The generation of $H3K4Me_3$ by histone lysine methyltransferase complexes (KMTs) that contains MLL1/2, ASH2L, BRBP5, WDR5, and other proteins leads to Wnt activation (Sierra et al., 2006). ASH2L interacts with β-catenin and recruits the MLL/1/2 complex to Wnt target genes (Gu et al., 2010). The methylation of H3K79 and H4K20 also correlates with Wnt activation. Dot1L, the mammalian homolog of Dot1 that is a SAM-dependent KMT, regulates the methylation of $H3K79Me_2$ and $H3K79Me_3$, and both of these methylated histones participates in Wnt activation (Mahmoudi et al., 2010). In the intestine, Dot1L undergoes recruitment to the TCF/β-catenin complex through its co-factor, AF10, and these events regulate Wnt signaling in intestinal stem cells. In addition to the MLL1/2 and Dot1L KMTs, Set8 regulates Wnt signaling through H4K20 mono-methylation (Li et al., 2011). Inhibitors for MLL1/2 (e.g., an MLL1/WDR5 inhibitor called MM-102 [Karatas et al., 2013]), Dot1L (e.g., EPZ-5676 [Daigle et al., 2013]), and Set8 (e.g., Ryuvidine [Blum et al., 2014]) are commercially available, but the initial expectations for these inhibitors as promising drugs for the treatment of leukemia are unfortunately offset by their limited effects on Wnt signaling and CRC proliferation, probably because of cell-type dependency or the redundancy of KMTs.

On the other hand, *demethylation events* by histone demethylases (KDMs) also regulate the levels and patterns of methylation and thereby affect chromatin remodeling and gene expression. Inhibition of KDMs may lead to a net increase in histone methylation patterns at specific lysine residues (Cloos et al., 2008; Jambhekar et al., 2017; Klose et al., 2006), leading, for example, to increased methylation of H3K9 or H3K27 that in turn represses transcription. The first reported KDM is LSD1 or KDM1A (Shi et al., 2004) that belongs, along with a related demethylase called KDM1B, to the so-called type 1 family of KDMs that contains a flavin adenine dinucleotide (FAD)-dependent amine oxidase (Jambhekar et al., 2017; Kooistra and Helin, 2012). The second type of KDMs contains a Jumonji C (JmjC) domain (Jambhekar et al., 2017; Klose et al., 2006) and embrace seven families of human JmjC domain-containing KDMs with specific demethylase activities (Klose et al., 2006; Kooistra and Helin, 2012). In the course of a program designed to develop new epigenetic regulators as antineoplastic agents (Sviripa et al., 2014; Zhang et al., 2013), we now report a family of carboxamide-substituted benzhydryl amines (CBAs) as KDM3A/3B inhibitors that selectively induce elevated levels of H3K9 methylation that in turn inhibit the Wnt signaling pathway in cell and zebrafish models.

RESULTS

High-Throughput Screening

To identify novel Wnt regulators by high-throughput screening, we assembled a stable HEK293T cell line containing the TOPFlash reporter (Zhang et al., 2019). Since mutations in the Wnt pathway often activated β-catenin, it was important to inhibit Wnt signaling *downstream* of β-catenin. We activated Wnt signaling by treating cells with lithium chloride that inhibited GSK3 and stabilized β-catenin (Hedgepeth et al., 1997), dual processes that mimicked the constitutively active Wnt signaling found in cancer cells. Starting from a compound library previously available from the Drug Discovery Center at University of Cincinnati (Cincinnati, OH, USA) as well as CBAs synthesized in-house using standard, chemical methodology, we identified CBA-1 that inhibited Wnt signaling at 500 nM concentrations.

To validate the screening results, we synthesized and purified CBA-1 (Figure 1A). Heating a 1:1 mixture of 4-(*N*,*N*-diethylamino)benzaldehyde and 5-chloroquinolin-8-ol with a 4-fold excess of butyramide at 130°C for 2 h and quenching with isopropanol furnished a precipitate of *N*-((5-chloro-8-hydroxyquinolin-7-yl) (4-(diethylamino)phenyl)-methyl)butyramide (CBA-1) (Figure 1A) in good yield and pure form, unlike commercial samples of CBA-1 that were contaminated with *ca.* 5% of an impurity, 7,7′-((4-(diethylamino)phenyl)methylene)bis (5-chloroquinolin-8-ol). This contaminant derived from the condensation of one equivalent of 4-(*N*,*N*-diethylamino)benzaldehyde with two equivalents of 5-chloroquinolin-8-ol.

We tested the activity of synthesized CBA-1 using TOPFlash reporter assay. Similar to the screening results, CBA-1 inhibited Wnt signaling induced by either LiCl or Wnt protein (Figure 1B). As a control, a well-known Wnt inhibitor, XAV939 (i.e., 3,5,7,8-tetrahydro-2-[4-(trifluoromethyl)phenyl]-4*H*-thiopyrano [4,3-*d*]

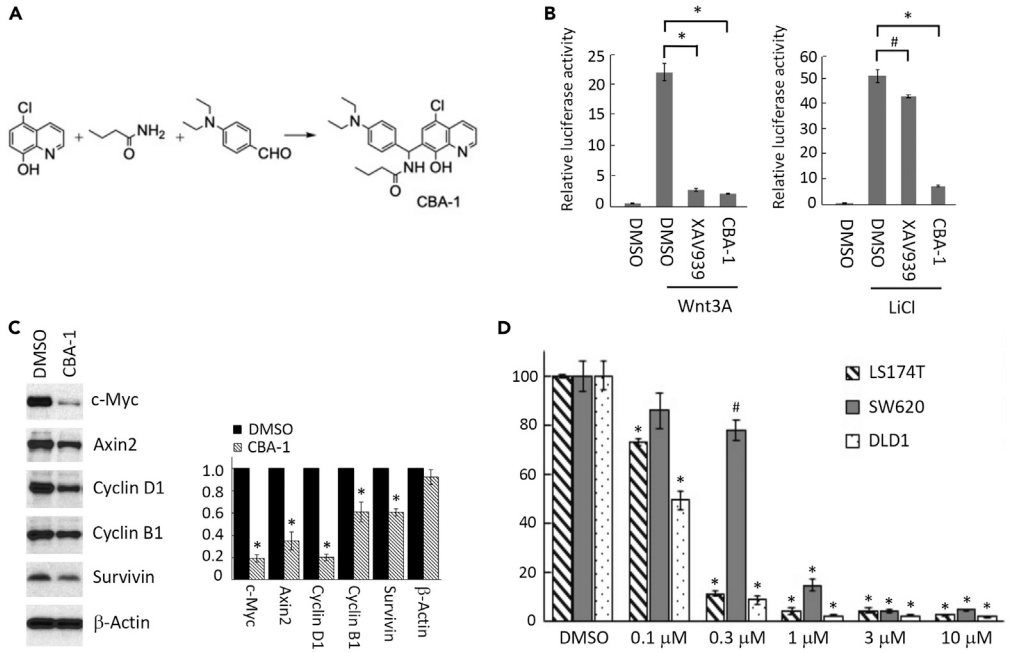

Figure 1. Validation of a Leading Wnt Inhibitor

(A) Synthesis of CBA-1 from 5-chloroquinolin-8-ol (1 eq), butyramide (4 eq), and 4-diethylaminobenzaldehyde (1 eq), 130°C, 2 h followed by the addition of isopropanol to induce precipitation (71% yield).

(B) Effects of CBA-1 (3 μM) and XAV939 (5 μM) on TOPFlash reporter activity (*$p < 0.0001$; #$p < 0.01$; $n = 3$).

(C) CBA-1 repressed Wnt target genes expression in LS174T CRC cells. Densitometry was analyzed using three western blot images (*$p < 0.05$; $n = 3$).

(D) CBA-1 inhibited CRC cell proliferation (*$p < 0.001$; #$p < 0.05$; $n = 3$).

pyrimidin-4-one, Sigma-Aldrich, MO), strongly inhibited Wnt-activated, but not LiCl-activated, TOPFlash reporter (Figure 1B), a result that indicated that CBA-1 and XAV939 have different mechanisms in inhibiting Wnt signaling. Treatment of LS174T CRC cells with CBA-1 repressed the expression of Wnt target genes (Figure 1C) and inhibited cell proliferation (Figure 1D), as expected given the importance of Wnt signaling in CRC.

XAV939 inhibited tankyrase, stabilized Axin, and promoted β-catenin degradation that thereby inhibited Wnt signaling. On the other hand, LiCl inhibited GSK3 that effected β-catenin phosphorylation and degradation and thereby activated Wnt signaling. When β-catenin *N*-terminal phosphorylation was blocked by either a serine/threonine mutation or GSK3 inhibitors, β-catenin became resistant to either XAV939- or Axin-induced degradation. Because CBA-1 inhibited LiCl-induced Wnt signaling, it was reasonable to assume that it inhibited Wnt signaling downstream of β-catenin, most likely by blocking β-catenin activity in the nucleus. To further analyze the activity of CBA-1, we treated mouse colon cancer organoids isolated from $Apc^{f/+}$/$Kras^{LSL-G12D}$/Villin-Cre mouse model (Figure S1A) (Wen et al., 2017). CBA-1 significantly inhibited colon cancer organoids formation (Figure S1B), suggesting that CBA-1 could inhibit colon cancer cells with APC and K-ras mutations.

CBA-1 Regulates Histone Methylation

CBA-1 showed no clear effects on the assembly of β-catenin/TCF (Figure 2A). Consequently, we hypothesized that CBA-1 inhibited Wnt signaling epigenetically by altering chromatin remodeling, and we probed the effects of CBA-1 on histone methylation. In both HEK293T and LS174T colorectal cancer cells, CBA-1 significantly increased the levels of $H3K9Me_2$ (Figures 2B and 2C) but had no effect on $H3K4Me_2$, outcomes that suggested that CBA-1 inhibited specific histone demethylase(s) and thereby promoted increased repressive methylation levels of histones and ultimately inhibited transcription. Indeed, chromatin immunoprecipitation (ChIP) assay with an anti-$H3K9Me_2$ Ab found that CBA-1 increased the levels of $H3K9Me_2$ on the promoters of Wnt target genes, c-Myc and Cyclin B1 (Figure 2D).

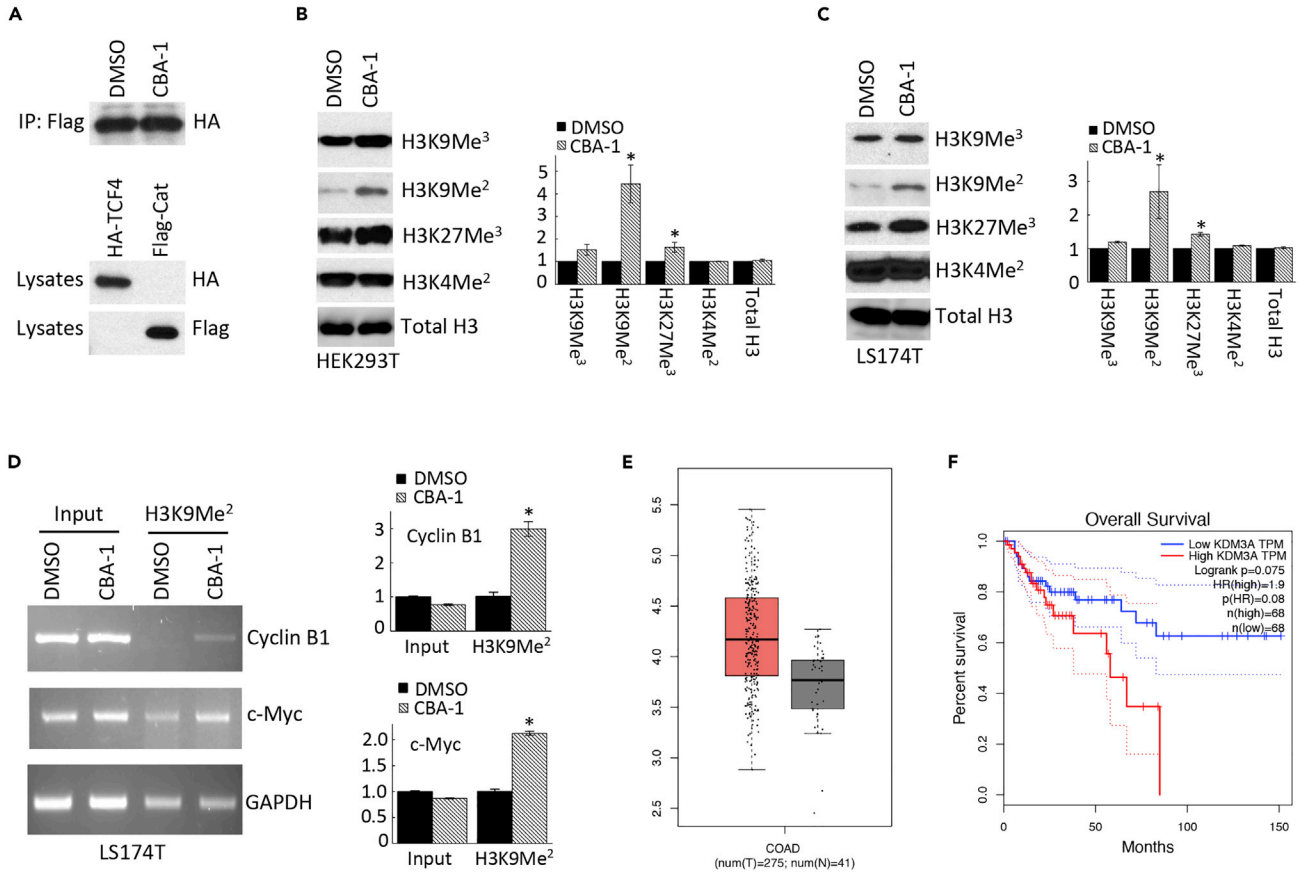

Figure 2. CBA-1 Regulates Histone Methylation

(A) CBA-1 did not inhibit the binding between β-catenin and TCF4. FLAG-tagged β-catenin and HA-tagged TCF4 were transfected separately into HEK293T cells. Equal amounts of β-catenin and TCF4 were mixed and immunoprecipitated by an anti-FLAG antibody. TCF4 was analyzed by an anti-HA antibody.

(B and C) CBA-1 significantly increased $H3K9Me_2$ and $H3K27Me_3$ in HEK293T and LS174T cells. Densitometry was analyzed using three western blot images (*$p < 0.05$; $n = 3$).to new sentences: (B) CBA-1 significantly increased $H3K9Me_2$ and $H3K27Me_3$ in HEK293T cells. Densitometry was analyzed using three western blot images (*$p < 0.05$; $n = 3$). (C) CBA-1 significantly increased $H3K9Me_2$ and $H3K27Me_3$ in LS174T cells. Densitometry was analyzed using three western blot images (*$p < 0.05$; $n = 3$).

(D) CBA-1 increased $H3K9Me_2$ on the promoters of Wnt target genes. The promoter sequences were analyzed by both standard PCR (left) and qPCR (right) (*$p < 0.01$; $n = 3$).

(E) KDM3A, a potential target of CBA-1, overexpressed in CRC. Tumor: red. Normal tissue: gray.

(F) High levels of KDM3A correlated with poor CRC patient survival.

Target Identification

Because it was reported that KDM3A regulated $H3K9Me_2$ in cancer cells (Li et al., 2017; Wang et al., 2019; Yoo et al., 2020), we analyzed the expression of KDM3A in CRC. The mRNA levels of KDM3A were upregulated in CRC (Figure 2E), and high levels of KDM3A expression also correlated with poor survival (Figure 2F). These findings suggested that KDM3A represented a previously unappreciated target for drug intervention in CRC. Because relatively few prior studies focused on KDM3A in CRC and because it has no specific FDA-approved inhibitor, we sought additional evidence to support the direct interaction of CBA-1 with KDM3A before launching additional synthetic, structure-activity relationship (SAR) studies.

Among the approaches for evaluating this direct interaction, we designed and synthesized biotinylated analogs of CBA-1 in which we attached D-biotin through a polyethylene glycol (PEG) spacer to the C-8 hydroxyl group in the 5-chloroquinolin-8-ol in CBA-B1 (Figure S2); the *N,N*-diethylamino group in CBA-B2 (Figure 3); and the carboxamide moiety in 4-(((5-chloro-8-hydroxyquinolin-7-yl) (4-morpholinophenyl) methyl)amino)-4-oxobutanoic acid in CBA-B3 (Figure S2). As a prerequisite for pull-down studies, we determined that CBA-B2 retained sufficient biological activity relative to CBA-1 as determined independently by evaluating Wnt inhibition (Figures 3A and 3B). A streptavidin-bead pull-down assay using HEK293T cell

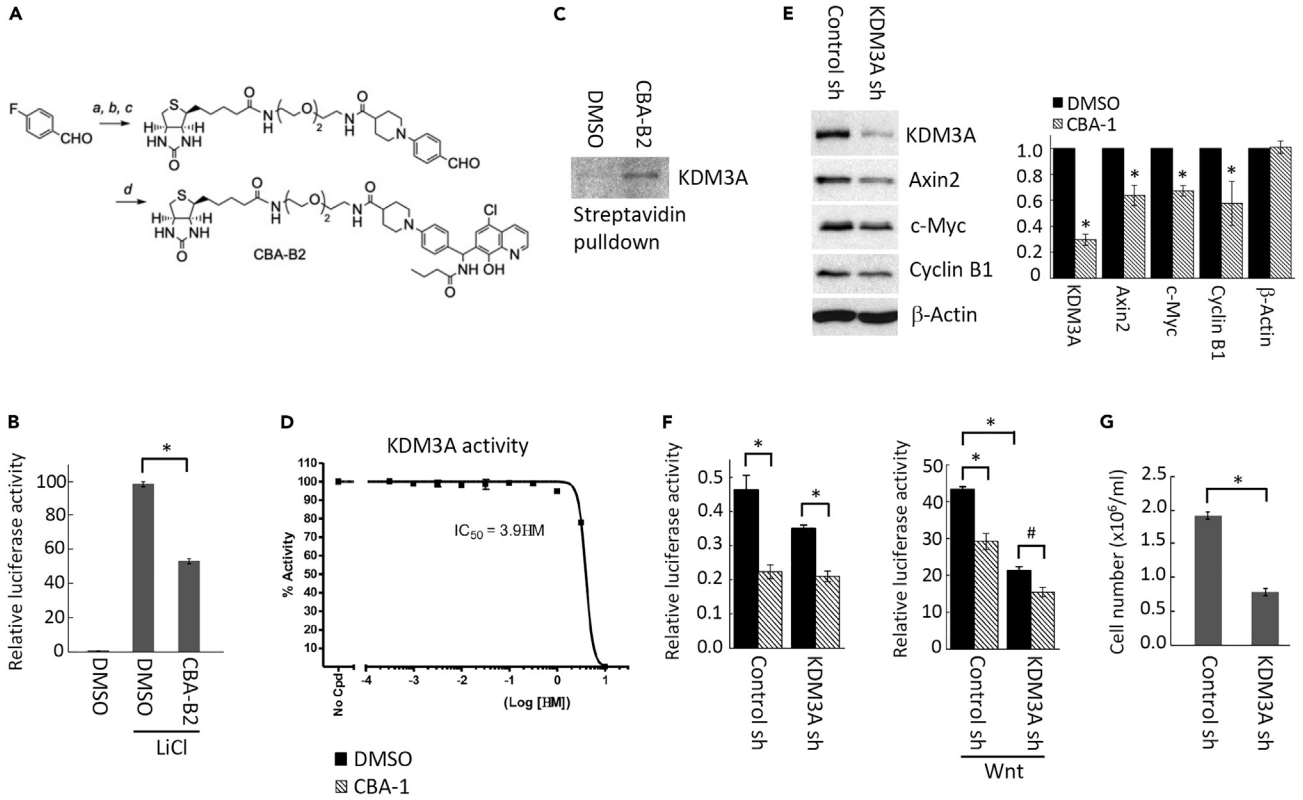

Figure 3. CBA-1 Interacts with KDM3A

(A) Synthesis of CBA-B2, a biological active biotinylated version of CBA-1; Legend: *a*, 4-fluorobenzaldehyde, ethyl piperidine-4-carboxylate, K_2CO_3, dimethyl sulfoxide, 120°C, 3 h (63% yield); *b*, 2 M NaOH, 48 h, 25°C (100% yield); *c*, *N*-(2-(2-(2-aminoethoxy)ethoxy)ethyl)-5-(2-oxohexahydro-1*H*-thieno [3,4-*d*]imidazol-4-yl)pentanamide (1 eq), 1-ethyl-3-(3-dimethylaminopropyl)carbodiimide hydrochloride (1.5 eq), 1-hydroxybenzotriazole (1.5 eq), triethylamine (1.5 eq), 12 h, 25°C (57% yield); *d*, 5-chloroquinolin-8-ol (1 eq), butyramide (6 eq), 150°C, 5 h (57% yield).

(B) CBA-B2 inhibited Wnt signaling (*$p < 0.0001$; $n = 3$).

(C) KDM3A was pulled down from HEK293T cell lysates by CBA-B2 and streptavidin beads.

(D) Dose-responses of CBA-1 on the enzymatic activities of KDM3A.

(E) Knocking down of KDM3A reduced Wnt target genes expression in LS174T CRC cells. Densitometry was analyzed using three western blot images (*$p < 0.05$; $n = 3$).

(F) Knocking down of KDM3A decreased Wnt-induced TOPFlash reporter activity (*$p < 0.01$; #$p < 0.05$; $n = 3$).

(G) Knocking down of KDM3A inhibited LS174T CRC cell proliferation (*$p < 0.0001$; $n = 3$).

lysates and CBA-B2 identified KDM3A as a binding partner (Figure 3C). After incubating the lysate with the streptavidin-CBA-B2-loaded beads, washing thoroughly, and evaluating the eluate by western blotting, we detected KDM3A, a finding that suggested that CBA-1 bound endogenous KDM3A. Consistent with this binding result, a dose-response study suggested that CBA-1 inhibited KDM3A activity *in vitro* at low micromolar levels (Figure 3D). Knocking down KDM3A by shRNA also inhibited Wnt target gene expression in LS174T CRC cells (Figure 3E) and inhibited Wnt-mediated TOPFlash reporter activity in HEK293T cells (Figure 3F), outcomes that validated KDM3A as a cancer-relevant target. These studies corroborated the CBA-1 inhibition of KDM3A as the key event in the observed Wnt inhibition. KDM3A shRNA also inhibited CRC cell proliferation (Figure 3G), a finding that linked *in vitro* inhibition of cell proliferation to the inhibition of Wnt signaling requiring KDM3A. These findings are consistent with a previous report that JMJD1A (KDM3A) promotes CRC growth and metastasis by enhancing Wnt signaling (Peng et al., 2018).

Molecular Modeling Studies

In the absence of an X-ray crystal structure of KDM3A, we turned to molecular modeling studies of a related histone demethylase. We utilized a BLAST search to determine that KDM3A exhibited 89% sequence similarity and 60% sequence identity to another family member, KDM3B (Figure S3A), that also possessed a

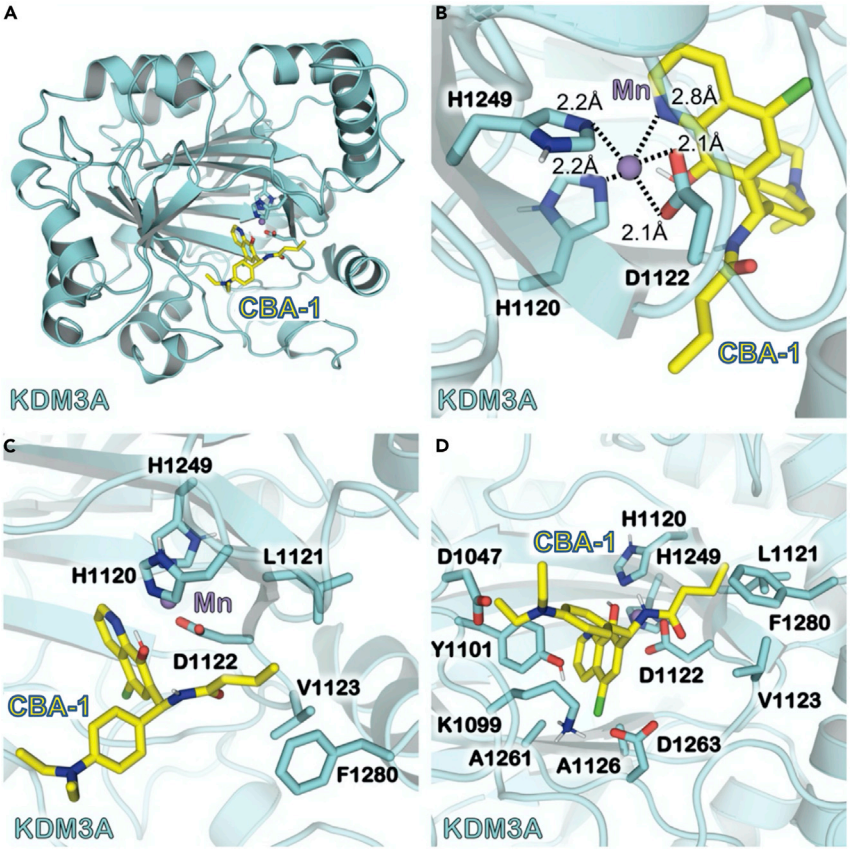

Figure 4. Molecular Modeling of the Binding Site of KDM3A with CBA-1

(A) Global view of the binding of CBA-1 to KDM3A. Cartoon model representations are shown of the KDM3A in cyan. CBA-1 is shown in stick model and colored yellow.

(B) Local view of the Mn^{2+}-binding site including CBA-1. Residues involved in the binding site are shown with stick model and colored the same color as its protein backbone. Dashed lines represent the coordination with distances shown close to the respective lines.

(C) Shown here is KDM3A with a focus on the hydrophobic interactions between CBA-1 and residues of KDM3A.

(D) Shown here is CBA-1 surrounded by residues of KDM3A that are within 4 Å of the inhibitor.

JmjC domain and that had a high-resolution crystal structure (PDB: 4C8D). We utilized molecular dynamics to construct a reasonable representation of KDM3A using the structure of KDM3B as a departure point. According to the RCSB database, the coordination of the manganese ion in the KDM3B active site involved water and *N*-oxalylglycine, and we assumed similar coordination in the modeled structure for KDM3A. In the homology model of KDM3A that emerged from these studies, the binding pose of the modeled structure of KDM3A (Figure 4A) predicted that CBA-1 coordinated directly to the Mn^{2+} ion site. An expanded view (Figure 4B) of the coordination of Mn^{2+} by CBA-1 showed that nitrogen of the quinoline ring in CBA-1 coordinated with the Mn^{2+} at 2.8 Å. The backbone atoms of KDM3A also coordinated with Mn^{2+}at 2.2 and 2.1 Å. We noted interesting hydrophobic interactions (Figure 4C) between portions of CBA-1 and residues L1120, V1123, and F1280 that resided within 4 Å of CBA-1. Finally, various polar and charged residues (Figure 4D) surrounded CBA-1 within 3 Å and defined the arrangement of functional groups in CBA-1 that provided the specificity seen in its binding to KMD3A. The binding pose shown in Figure 4 has a binding free energy of −12.3 kcal/mol.

The JmjC domains of KDM3A and KDM3B are very similar (Figure S3A). CBA-1 also inhibited KDM3B (Figure S3B), but the inhibition activity for KDM3B was poorer than its inhibition activity for KDM3A (Figure 3D). We also analyzed the binding pose of the inhibitor CBA-1 with the crystal structure of KDM3B (Figure S3C). The global view of the structure suggested that the inhibitor bound and coordinated with Mn^{2+} in the JmjC

domain. The CBA-1 inhibitor and the three residues from KDM3B coordinated with the manganese cation (Figure S3D). A delta nitrogen from H1689 and H1560 of KDM3B coordinated with Mn^{2+} at 2.3 Å. A third residue, namely, D1562 of KDM3B, coordinated with Mn^{2+} through two oxygens from the carboxylic group at 2.1 Å. Lastly, the inhibitor CBA-1 coordinates with Mn^{2+} through a cyclic nitrogen at 3.9 Å. Neighboring residues of KDM3B promoted the binding of the inhibitor to the domain with hydrophobic and basic side-chain interactions (Figure S3E). These residues are F1720, I1683, and H1648, which can be found to be within 3 Å of CBA-1 (Figure S3F); no other important interactions between CBA-1 and KDM3B were noted.

Although a specific KDM3A inhibitor was not available commercially, other KDM inhibitors target the JmjC domain. For example, GSK-J1 and GSK-J4 were originally described as specific inhibitors for H3K27 demethylases JMJD3/KDM6B (UTX) (Kruidenier et al., 2012). Further studies found that these KDM inhibitors in fact had broad activities in inhibiting JmjC domain in KDMs, probably with differential preferences for different KDMs (Heinemann et al., 2014). We found, for example, that GSK-J4, but not GSK-J1, inhibited Wnt signaling (Figure S4), a finding that suggested that GSK-J4 like CBA-1 also inhibited KDM3A. GSK-J1 was not active in this cell-based assay, possibly because of its restricted cell permeability (Kruidenier et al., 2012). However, the facile absorption and metabolism of GSK-J4 to GSK-J1 in the cells (Kruidenier et al., 2012) suggested GSK-J1 is the actual, active KDM3A inhibitor.

We also analyzed the binding pose of the inhibitor GSK-J1 with the modeled structure of KDM3A (Figures 4 and S5) that we developed. A global view of the protein with the Mn^{2+} ion and GSK-J1 (Figure S5A) showed that GSK-J1 bound to KDM3A at the Mn^{2+}-binding site with coordination between GSK-J1 and the Mn^{2+} ion (Figure S5B). A nitrogen from GSK-J1 coordinated with the Mn^{2+} ion at a distance of 2.8 Å. KDM3A residues coordinated with Mn^{2+} at 2.2 and 2.1 Å. There were no other important interactions between GSK-J1 and KDM3A other than the coordination with Mn^{2+} as shown in alternate views of surrounding residues within 3 Å of GSK-J1 (Figures S5C and S5D). The binding pose for this structure in Figure S5 has a binding free energy of −6.6 kcal/mol. The binding affinity of CBA-1 to KDM3A is greater than that of GSK-J1, a finding consistent with the TOPFlash reporter assay that indicated that CBA-1 was a better Wnt inhibitor than either GSK-J1 or GSK-J4 (Figure S4B).

In Vivo Studies with CBA-1

To validate the *in vivo* activity of CBA-1, we employed a Wnt/β-catenin zebrafish reporter line, Tcf/Lef-miniP:dGFP(Scaffidi et al., 2002), in which GFP expression occurred mostly in the tail of the larvae where Wnt signaling is active during development (Figure 5A). The effects of CBA-1 on GFP expression were analyzed using the following agents: DMSO (vehicle) and GSK3 inhibitor called Bio (6-bromoindirubin-3′-oxime, Sigma-Aldrich, MO, USA). CBA-1 inhibited Wnt signaling in the tail (Figure 5B). As a control, Bio inhibited GSK3, stabilized β-catenin, and thus activated Wnt signaling (Figure 5C). Wnt signaling is also critical for zebrafish tail fin regeneration after amputation. CBA-1 treatment reduced Wnt-dependent tail regeneration in amputated tails of adult Tcf/Lef-miniP:dGFP zebrafish and led to a decrease in GFP expression at the regenerating edge of the tail fin compared with DMSO control (Figures 5F–5L). Since some compounds may affect the reporter or tail fin regeneration through nonspecific or even toxic effects, we performed an eye rescue experiment to further test if CBA-1 specifically inhibits the Wnt signaling in zebrafish (Figures 5D and 5E). Wnt signaling also mediates eye development in zebrafish, in which excessive Wnt signaling has deleterious effects in early embryos. Bio treatment resulted in a "no-eye" phenotype in zebrafish embryos, CBA-1 rescued Bio-induced eye defects (Figure 5D), and CBA-1 rescued Bio-induced eye defects in a dose-responsive manner (Figure 5E). At both 5 and 10 μM concentrations, CBA-1 was able to rescue completely the loss-of-eye phenotype. Additionally, we observed no obvious toxicity or embryo deaths with up to 20 μM concentrations of CBA-1.

DISCUSSION

The inhibition of Wnt signaling is an important goal for the development of new therapeutics for colon cancer treatment (Anastas and Moon, 2013; Nusse and Clevers, 2017). Histone acetylases and histone methyltransferases play central roles in chromatin remodeling and hence transcriptional activation of Wnt target genes. Small-molecule inhibitors that target these epigenetic mechanisms are attractive agents for regulating transcription and developing new antineoplastic drugs, particularly in the case of CRC where Wnt signaling is important (Patnaik and Anupriya, 2019; Polakis, 2012). In this study, we identified *N*-((5-chloro-8-hydroxyquinolin-7-yl) (4-(diethylamino)phenyl)-methyl)butyramide (CBA-1), a representative member of a family of small-molecule, epigenetic Wnt inhibitors for a specific histone demethylase,

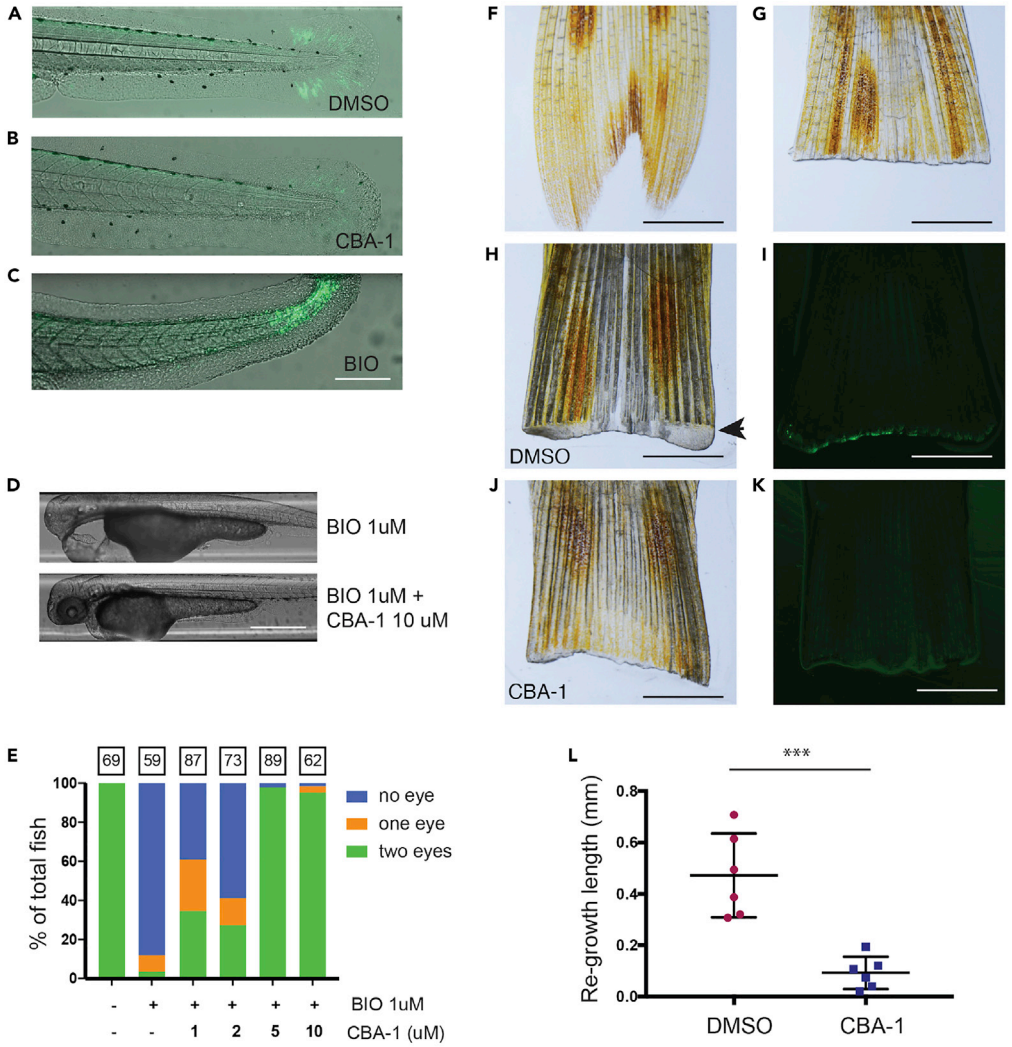

Figure 5. CBA-1 Inhibited Wnt Signaling in Zebrafish Models

(A) TCF/LEF-GFP zebrafish model. GFP was expressed in the tails where there is active Wnt signaling.

(B) CBA-1 (10 μM) inhibited GFP expression in the tails.

(C) Bio (1 μM), a GSK3 inhibitor and Wnt activator, significantly induced GFP expression in the TCF/LEF-GFP zebrafish model. Scale bar, 0.25 mm.

(D) Representative images of no eye phenotype seen with Bio (1 μM) treatment and eye rescue phenotype seen with Bio (1 μM) + CBA-1 (10 μM) treatment. Scale bar, 0.5 mm.

(E) Eye development assay. Wnt activation by Bio inhibited eye development (no eye phenotype). CBA-1 inhibited Bio-induced Wnt signaling, leading to partial (one eye) or full (two eyes) rescue of the eye development in a dose-dependent manner. Numbers above bars represent total number of fish per group.

(F) Uncut tail of TCF/LEF GFP sheer zebrafish. Scale bar, 2 mm.

(G) Tail immediately post amputation.

(H and I) Partial tail regeneration and GFP fluorescence were observed in DMSO-treated zebrafish. Arrowhead depicts tail regeneration.

(J and K) A complete loss of GFP fluorescence and lack of tail regeneration were observed in CBA-1 (5 μM)-treated fish.

(L) CBA-1 treatment leads to a significant decrease in length of tail regeneration. ***p = 0.0003.

KDM3A, that foreclosed on Wnt signaling by increasing histone methylation at H3K9, a repression marker for gene transcription.

A high-throughput screening program using a stable cell line containing a TOPFlash reporter first identified this carboxyamide-substituted benzhydryl amine CBA-1 as a Wnt signaling inhibitor. We compared

CBA-1 with XAV939, a well-known tankyrase inhibitor that regulated β-catenin stability. CBA-1 significantly inhibited LiCl-induced Wnt signaling, suggesting that CBA-1 did not affect β-catenin stability but inhibited β-catenin activity (Figure 1B). CBA-1 also had no effects on β-catenin/TCF/complex (Figure 2A), a finding that indicated that CBA-1 inhibited Wnt signaling by affecting chromatin remodeling. We analyzed different histone methylation markers and found that CBA-1 induced histone methylation on H3K9Me_2 (Figures 2B–2D) that controlled transcriptional silencing. A biologically active, biotinylated variant, namely, CBA-B2 (Figures 3A–3C), led to a successful pull-down experiment that confirmed KDM3A as the target of CBA-1. Additional validation of this outcome emerged from shRNA suppression of KDM3A that inhibited, as expected, Wnt signaling (Figures 3E–3G) and pointed to KDM3A as a crucial regulatory element in the Wnt signaling pathway.

Although we identified KDM3A as a direct target of CBA-1 and an important regular of Wnt signaling, we do not expect that KDM3A only regulates Wnt signaling. As we know, the well-established Wnt inhibitor XAV939 targets tankyrase (Huang et al., 2009) and ICG-001 targets CBP (Emami et al., 2004). These enzymes regulate many proteins and are also not specific for Wnt signaling. However, our findings suggested that Wnt signaling can be efficiently inhibited by small-molecule KDM3A inhibitors, such as CBA-1. CBA-1 inhibited colon cancer cells with APC or β-catenin mutations (Figure 1D) and also inhibited colon cancer organoids with APC and K-ras mutation (Figure S1B). KDM3A was overexpressed in CRC, and the expression levels of KDM3A inversely correlated with patient survival (Figures 2E and 2F). KDM3A is required for both growth and metastasis of CRC (Peng et al., 2018), further suggesting that KDM3A is an important target for CRC treatment.

We recognize that KDM3A may not be the only target and structural variations in CBA-1 may affect other JmjC domain-containing histone demethylases, particularly other members of KDM3 (Li et al., 2017). As demonstrated in Figure 3F, CBA-1 further decreased the Wnt reporter activity inhibited by KDM3A shRNA, suggesting that CBA-1 may inhibit other KMD (s) that also regulate the Wnt signaling. Indeed, CBA-1 inhibited KDM3B activity as well (Figure S3). We also recognize that inhibitors for other histone demethylases, structurally unrelated to CBA-1, may also inhibit KDM3A through binding events at locales other than the site identified in our molecular modeling study. For example, we compared the KDM6 inhibitors GSK-J1/J4 with CBA-1. Although less potent that CBA-1, GSK-J1/J4 also inhibited Wnt signaling (Figure S4). Docking studies suggest that CBA-1 and GSK-J1 coordinated the manganese Mn^{2+} ion in the active site of KDM3A, but CBA-1 has additional hydrophobic interactions with residues L1120, V1123, and F1280 and thus exhibited a much higher binding affinity (Figures 4 and S5) than the binding affinity of GSK-J1. The docking study explained the finding that CBA-1 was superior to GSK-J1/J4 in KDM3A/Wnt inhibition (Figures S4 and S5). CBA-1 coordinated with Mn^{2+} at a long distance in KDM3B (3.9 Å) than the distance in KDM3A (2.8 Å) (Figures 4 and S3). This could be one of the reasons that CBA-1 inhibited KDM3A more significantly than KDM3B.

To test the activity of CBA-1 *in vivo*, we utilized a zebrafish Wnt/β-catenin reporter line that indicated that CBA-1 inhibited Wnt-mediated GFP expression in the tails where the Wnt pathway was most active (Figure 5). CBA-1 inhibited tail fin regeneration, a process regulated by Wnt signaling. During embryogenesis, excess Wnt signaling also blocked eye development in zebrafish. CBA-1 rescued the "no-eye phenotype" induced by a Wnt activator Bio with no toxicity to developing animals, an important observation that suggested that CBA-1 specifically inhibited Wnt signaling *in vivo* and that also suggested that CBA-1 is a promising leading compound for the development of clinically useful Wnt inhibitors. These zebrafish models provide high-throughput methods to screen Wnt inhibitors and to test the toxicity of drug candidates *in vivo*.

Given the high similarity of the KDM structures, particularly the JmjC domains, development of small-molecule inhibitors that target only a specific JmjC domain-containing KDM remains as a scientific challenge. For example, GSK-J1/J4 were originally developed as specific KDM6 inhibitors (Kruidenier et al., 2012) but were later reported as broad KDM inhibitors (Heinemann et al., 2014). Other reported "specific" KDM inhibitors may also have multiple targets. As we discussed above, CBA-1 may also inhibit other JmjC domain-containing KDMs that regulate H3K9 methylation and Wnt signaling. In addition, CBA-1 increased H3K27 methylation (Figures 2B and 2C), suggesting that it may inhibit cancer cell growth by targeting multiple JmjC domain-containing KDMs. Although a highly specific inhibitor that only targets a single enzyme is often prized as a molecular probe, an inhibitor that targets a family of functionally redundant

enzymes has value in therapeutic drug development. Epigenetic drugs targeting a subfamily of KDMs may be a more efficient approach for cancer treatment. CBA-1 not only inhibited Wnt signaling in cancer cells but may also inhibit Wnt signaling in normal cells (Figure 3F), suggesting that it may have potential toxic effects in animals and should be further optimized through structure-activity relationship (SAR) studies. Nonetheless, the identification of CBA-1 as KDM3A and KDM3B inhibitors and the utility of molecular modeling of CBAs in the KMD3A/3B construct provide the means for structure-guided, future SAR studies that will develop CBA inhibitors targeting specific KDMs for Wnt inhibition and cancer treatment.

Limitations of the Study

In this study, we developed a family of carboxamide-substituted benzhydryl amines (CBAs) as histone lysine demethylase (KDM) inhibitors. Specifically, we found that CBA-1 inhibited KDM3A/3B and increased the levels of $H3K9Me_2$. We also found that CBA-1 inhibited Wnt signaling *in vitro* in colon cancer cells and *in vivo* in zebrafish models. However, the specificity of CBA-1 on different KDMs should be further examined in the future. It is also important to perform additional SAR studies to further optimize CBA-1 for future clinical development.

Resource Availability

Lead Contact

Further information and requests should be directed to the Lead Contact, Professor Chunming Liu (chunming.liu@uky.edu)

Materials Availability

Materials are available from the corresponding authors on request.

Data and Code Availability

This study did not generate computer code. All data and analytical methods are available in the main text or in Supplemental Information.

METHODS

All methods can be found in the accompanying Transparent Methods supplemental file.

SUPPLEMENTAL INFORMATION

Supplemental Information can be found online at https://doi.org/10.1016/j.isci.2020.101795.

ACKNOWLEDGMENTS

We are grateful to Professor Randall Moon for the Super 8× TOPFlash and 8× FOPFlash plasmids and Professor Tianyan Gao for mouse colon cancer organoids. C.L. and D.S.W. were supported by NIH R01 CA172379 from the National Institutes of Health and by NIH UL1 TR000117 from the National Institutes of Health to the University of Kentucky's Center for Clinical and Translational Science. D.S.W. was also supported in part by the Office of the Dean of the College of Medicine, the Center for Pharmaceutical Research and Innovation in the College of Pharmacy, the Department of Defense (DoD) Prostate Cancer Research Program Award W81XWH-16-1-0635 [Grant Log# PC150326P2], and NIH P30 RR020171 from the National Institute of General Medical Sciences to L. Hersh. V.M.S. was supported by grant IRG 16-182-28 from the American Cancer Society. J.S.B. and M.G.H. are supported by NIH R37 CA227656 and T32 CA165990, respectively. This study is also supported by Markey Cancer Center (P30 CA177558).

AUTHOR CONTRIBUTIONS

Conceptualization, C.L. and D.S.W.; Methodology, W.Z., V.M.S., Y.X., T.Y., and M.G.H.; Data Analysis, W.Z., V.M.S., J.S.B., and C.-G.Z.; Supervision, C.L., D.S.W., J.S.B., and C.-G.Z.; Writing, C.L. and D.S.W.

DECLARATION OF INTERESTS

C.L. and D.S.W. have partial ownership in a for-profit venture, Epionc, Inc., that seeks to develop small-molecule inhibitors for cancer treatment. In accord with University of Kentucky policies, C.L. and D.S.W.

have disclosed this work to the University of Kentucky's Intellectual Property Committee and to a Conflict of Interest Oversight Committee in accord with University of Kentucky policies.

Received: July 13, 2020
Revised: September 24, 2020
Accepted: November 9, 2020
Published: December 18, 2020

REFERENCES

Anastas, J.N., and Moon, R.T. (2013). WNT signalling pathways as therapeutic targets in cancer. Nat. Rev. Cancer *13*, 11–26.

Barker, N., and Clevers, H. (2006). Mining the Wnt pathway for cancer therapeutics. Nat. Rev. Drug Discov. *5*, 997–1014.

Blum, G., Ibanez, G., Rao, X., Shum, D., Radu, C., Djaballah, H., Rice, J.C., and Luo, M. (2014). Small-molecule inhibitors of SETD8 with cellular activity. ACS Chem. Biol. *9*, 2471–2478.

Chen, B., Dodge, M.E., Tang, W., Lu, J., Ma, Z., Fan, C.W., Wei, S., Hao, W., Kilgore, J., Williams, N.S., et al. (2009). Small molecule-mediated disruption of Wnt-dependent signaling in tissue regeneration and cancer. Nat. Chem. Biol. *5*, 100–107.

Cloos, P.A., Christensen, J., Agger, K., and Helin, K. (2008). Erasing the methyl mark: histone demethylases at the center of cellular differentiation and disease. Genes Dev. *22*, 1115–1140.

Daigle, S.R., Olhava, E.J., Therkelsen, C.A., Basavapathruni, A., Jin, L., Boriack-Sjodin, P.A., Allain, C.J., Klaus, C.R., Raimondi, A., Scott, M.P., et al. (2013). Potent inhibition of DOT1L as treatment of MLL-fusion leukemia. Blood *122*, 1017–1025.

Emami, K.H., Nguyen, C., Ma, H., Kim, D.H., Jeong, K.W., Eguchi, M., Moon, R.T., Teo, J.L., Kim, H.Y., Moon, S.H., et al. (2004). A small molecule inhibitor of beta-catenin/CREB-binding protein transcription [corrected]. Proc. Natl. Acad. Sci. U S A *101*, 12682–12687.

Feng, M., Jin, J.Q., Xia, L., Xiao, T., Mei, S., Wang, X., Huang, X., Chen, J., Liu, M., Chen, C., et al. (2019). Pharmacological inhibition of beta-catenin/BCL9 interaction overcomes resistance to immune checkpoint blockades by modulating Treg cells. Sci. Adv. *5*, eaau5240.

Garber, K. (2009). Drugging the Wnt pathway: problems and progress. J. Natl. Cancer Inst. *101*, 548–550.

Greer, E.L., and Shi, Y. (2012). Histone methylation: a dynamic mark in health, disease and inheritance. Nat. Rev. Genet. *13*, 343–357.

Gu, B., Watanabe, K., and Dai, X. (2010). Epithelial stem cells: an epigenetic and Wnt-centric perspective. J. Cell Biochem. *110*, 1279–1287.

Hedgepeth, C.M., Conrad, L.J., Zhang, J., Huang, H.C., Lee, V.M., and Klein, P.S. (1997). Activation of the Wnt signaling pathway: a molecular mechanism for lithium action. Dev. Biol. *185*, 82–91.

Heinemann, B., Nielsen, J.M., Hudlebusch, H.R., Lees, M.J., Larsen, D.V., Boesen, T., Labelle, M., Gerlach, L.O., Birk, P., and Helin, K. (2014). Inhibition of demethylases by GSK-J1/J4. Nature *514*, E1–E2.

Huang, S.M., Mishina, Y.M., Liu, S., Cheung, A., Stegmeier, F., Michaud, G.A., Charlat, O., Wiellette, E., Zhang, Y., Wiessner, S., et al. (2009). Tankyrase inhibition stabilizes axin and antagonizes Wnt signalling. Nature *461*, 614–620.

Hyun, K., Jeon, J., Park, K., and Kim, J. (2017). Writing, erasing and reading histone lysine methylations. Exp. Mol. Med. *49*, e324.

Jambhekar, A., Anastas, J.N., and Shi, Y. (2017). Histone lysine demethylase inhibitors. Cold Spring Harb. Perspect. Med. *7*, a026484.

Karatas, H., Townsend, E.C., Cao, F., Chen, Y., Bernard, D., Liu, L., Lei, M., Dou, Y., and Wang, S. (2013). High-affinity, small-molecule peptidomimetic inhibitors of MLL1/WDR5 protein-protein interaction. J. Am. Chem. Soc. *135*, 669–682.

Kinzler, K.W., and Vogelstein, B. (1996). Lessons from hereditary colorectal cancer. Cell *87*, 159–170.

Klose, R.J., Kallin, E.M., and Zhang, Y. (2006). JmjC-domain-containing proteins and histone demethylation. Nat. Rev. Genet. *7*, 715–727.

Kooistra, S.M., and Helin, K. (2012). Molecular mechanisms and potential functions of histone demethylases. Nat. Rev. Mol. Cell. Biol. *13*, 297–311.

Kruidenier, L., Chung, C.W., Cheng, Z., Liddle, J., Che, K., Joberty, G., Bantscheff, M., Bountra, C., Bridges, A., Diallo, H., et al. (2012). A selective jumonji H3K27 demethylase inhibitor modulates the proinflammatory macrophage response. Nature *488*, 404–408.

Lee, E., Madar, A., David, G., Garabedian, M.J., Dasgupta, R., and Logan, S.K. (2013). Inhibition of androgen receptor and beta-catenin activity in prostate cancer. Proc. Natl. Acad. Sci. U S A *110*, 15710–15715.

Lenz, H.J., and Kahn, M. (2014). Safely targeting cancer stem cells via selective catenin coactivator antagonism. Cancer Sci. *105*, 1087–1092.

Lepourcelet, M., Chen, Y.N., France, D.S., Wang, H., Crews, P., Petersen, F., Bruseo, C., Wood, A.W., and Shivdasani, R.A. (2004). Small-molecule antagonists of the oncogenic Tcf/beta-catenin protein complex. Cancer Cell *5*, 91–102.

Li, J., Yu, B., Deng, P., Cheng, Y., Yu, Y., Kevork, K., Ramadoss, S., Ding, X., Li, X., and Wang, C.Y. (2017). KDM3 epigenetically controls tumorigenic potentials of human colorectal cancer stem cells through Wnt/beta-catenin signalling. Nat. Commun. *8*, 15146.

Li, Z., Nie, F., Wang, S., and Li, L. (2011). Histone H4 Lys 20 monomethylation by histone methylase SET8 mediates Wnt target gene activation. Proc. Natl. Acad. Sci. U S A *108*, 3116–3123.

Liu, C., Kato, Y., Zhang, Z., Do, V.M., Yankner, B.A., and He, X. (1999). beta-Trcp couples beta-catenin phosphorylation-degradation and regulates Xenopus axis formation. Proc. Natl. Acad. Sci. U S A *96*, 6273–6278.

Liu, C., Li, Y., Semenov, M., Han, C., Baeg, G.H., Tan, Y., Zhang, Z., Lin, X., and He, X. (2002). Control of beta-catenin phosphorylation/degradation by a dual-kinase mechanism. Cell *108*, 837–847.

Liu, J., Pan, S., Hsieh, M.H., Ng, N., Sun, F., Wang, T., Kasibhatla, S., Schuller, A.G., Li, A.G., Cheng, D., et al. (2013). Targeting Wnt-driven cancer through the inhibition of porcupine by LGK974. Proc. Natl. Acad. Sci. U S A *110*, 20224–20229.

Lyou, Y., Habowski, A.N., Chen, G.T., and Waterman, M.L. (2017). Inhibition of nuclear Wnt signalling: challenges of an elusive target for cancer therapy. Br. J. Pharmacol. *174*, 4589–4599.

Mahmoudi, T., Boj, S.F., Hatzis, P., Li, V.S., Taouatas, N., Vries, R.G., Teunissen, H., Begthel, H., Korving, J., Mohammed, S., et al. (2010). The leukemia-associated Mllt10/Af10-Dot1l are Tcf4/beta-catenin coactivators essential for intestinal homeostasis. PLoS Biol. *8*, e1000539.

Nusse, R., and Clevers, H. (2017). Wnt/beta-Catenin signaling, disease, and emerging therapeutic modalities. Cell *169*, 985–999.

Patnaik, S., and Anupriya. (2019). Drugs targeting epigenetic modifications and plausible therapeutic strategies against colorectal cancer. Front. Pharmacol. *10*, 588.

Peng, K., Su, G., Ji, J., Yang, X., Miao, M., Mo, P., Li, M., Xu, J., Li, W., and Yu, C. (2018). Histone demethylase JMJD1A promotes colorectal cancer growth and metastasis by enhancing Wnt/beta-catenin signaling. J. Biol. Chem. *293*, 10606–10619.

Polakis, P. (2012). Wnt signaling in cancer. Cold Spring Harb. Perspect. Biol. *4*, a008052.

Scaffidi, P., Misteli, T., and Bianchi, M.E. (2002). Release of chromatin protein HMGB1 by necrotic cells triggers inflammation. Nature *418*, 191–195.

Schneider, J.A., Craven, T.W., Kasper, A.C., Yun, C., Haugbro, M., Briggs, E.M., Svetlov, V., Nudler,

E., Knaut, H., Bonneau, R., et al. (2018). Design of peptoid-peptide macrocycles to inhibit the beta-catenin TCF interaction in prostate cancer. Nat. Commun. *9*, 4396.

Shi, Y., Lan, F., Matson, C., Mulligan, P., Whetstine, J.R., Cole, P.A., Casero, R.A., and Shi, Y. (2004). Histone demethylation mediated by the nuclear amine oxidase homolog LSD1. Cell *119*, 941–953.

Sierra, J., Yoshida, T., Joazeiro, C.A., and Jones, K.A. (2006). The APC tumor suppressor counteracts beta-catenin activation and H3K4 methylation at Wnt target genes. Genes Dev. *20*, 586–600.

Sviripa, V.M., Zhang, W., Balia, A.G., Tsodikov, O.V., Nickell, J.R., Gizard, F., Yu, T., Lee, E.Y., Dwoskin, L.P., Liu, C., and Watt, D.S. (2014). 2′,6′-Dihalostyrylanilines, pyridines, and pyrimidines for the inhibition of the catalytic subunit of methionine S-adenosyltransferase-2. J. Med. Chem. *57*, 6083–6091.

Wang, H.Y., Long, Q.Y., Tang, S.B., Xiao, Q., Gao, C., Zhao, Q.Y., Li, Q.L., Ye, M., Zhang, L., Li, L.Y., and Wu, M. (2019). Histone demethylase KDM3A is required for enhancer activation of hippo target genes in colorectal cancer. Nucleic Acids Res. *47*, 2349–2364.

Wen, Y.A., Xing, X., Harris, J.W., Zaytseva, Y.Y., Mitov, M.I., Napier, D.L., Weiss, H.L., Mark Evers, B., and Gao, T. (2017). Adipocytes activate mitochondrial fatty acid oxidation and autophagy to promote tumor growth in colon cancer. Cell Death Dis. *8*, e2593.

Wisniewski, J.A., Yin, J., Teuscher, K.B., Zhang, M., and Ji, H. (2016). Structure-based design of 1,4-dibenzoylpiperazines as beta-catenin/B-cell lymphoma 9 protein-protein interaction inhibitors. ACS Med. Chem. Lett. *7*, 508–513.

Yang, J., Zhang, W., Evans, P.M., Chen, X., He, X., and Liu, C. (2006). Adenomatous polyposis coli (APC) differentially regulates beta-catenin phosphorylation and ubiquitination in colon cancer cells. J. Biol. Chem. *281*, 17751–17757.

Yoo, J., Jeon, Y.H., Cho, H.Y., Lee, S.W., Kim, G.W., Lee, D.H., and Kwon, S.H. (2020). Advances in histone demethylase KDM3A as a cancer therapeutic target. Cancers (Basel) *12*, 1098.

Zhang, W., Sviripa, V., Chen, X., Shi, J., Yu, T., Hamza, A., Ward, N.D., Kril, L.M., Vander Kooi, C.W., Zhan, C.G., et al. (2013). Fluorinated N,N-dialkylaminostilbenes repress colon cancer by targeting methionine S-adenosyltransferase 2A. ACS Chem. Biol. *8*, 796–803.

Zhang, W., Sviripa, V.M., Kril, L.M., Yu, T., Xie, Y., Hubbard, W.B., Sullivan, P.G., Chen, X., Zhan, C.G., Yang-Hartwich, Y., et al. (2019). An underlying mechanism of dual Wnt inhibition and AMPK activation: mitochondrial uncouplers masquerading as Wnt inhibitors. J. Med. Chem. *62*, 11348–11358.

Zhong, Z., and Virshup, D.M. (2020). Wnt signaling and drug resistance in cancer. Mol. Pharmacol. *97*, 72–89.

iScience, Volume *23*

Supplemental Information

Epigenetic Regulation of Wnt Signaling by Carboxamide-Substituted Benzhydryl Amines that Function as Histone Demethylase Inhibitors

Wen Zhang, Vitaliy M. Sviripa, Yanqi Xie, Tianxin Yu, Meghan G. Haney, Jessica S. Blackburn, Charles A. Adeniran, Chang-Guo Zhan, David S. Watt, and Chunming Liu

Supplemental Information

Epigenetic Regulation of Wnt Signaling by Carboxamide-substituted Benzhydryl Amines That Function as Histone Demethylase Inhibitors

Wen Zhang, Vitaliy M. Sviripa, Yanqi Xie, Tianxin Yu, Meghan G. Haney,

Jessica S. Blackburn, Charles A. Adeniran, Chang-Guo Zhan,

David S. Watt, and Chunming Liu

SUPPLEMENTAL FIGURES

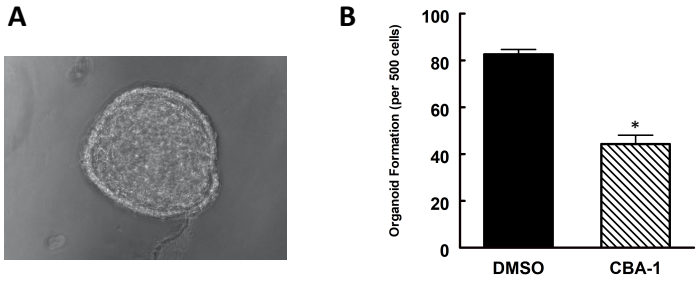

Figure S1. Effects of CBA-1 on colon cancer organoids. Related to Figure 1.

A. Colon cancer organoids from $Apc^{f/+}$/$Kras^{LSL\text{-}G12D}$/Villin-Cre mouse model. **B. CBA-1** (3 μM) inhibited colon cancer organoids formation (* $p < 0.01$; $n = 3$).

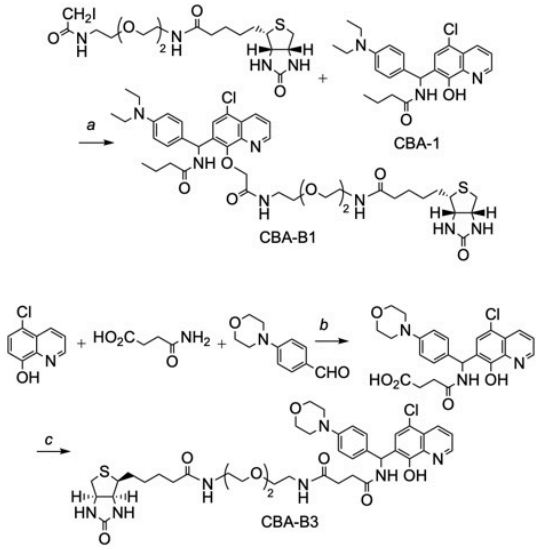

Figure S2. Biotinylated CBAs. Related to Figure 3.

Synthesis of additional biotinylated analogs of **CBA-1**. Synthesis of **CBA-B1**. Legend: *a*, CBA-1 (1 eq), *N*-(2-(2-(2-iodoacetamido)ethoxy)ethyl)-5-((*3aS,4S,6aR*)-2-oxohexahydro-1*H*-thieno[3,4-*d*]imidazol-4-yl)pentanamide (1 eq), K_2CO_3 (1.3 eq), dimethylformamide, 80°C, 3 h (20% yield). Synthesis of **CBA-B2** displayed in **Fig. 3**. Synthesis of **CBA-B3**. Legend: *b*, 5-chloroquinolin-8-ol (1 eq), 4-amino-4-oxobutanoic acid (1 eq), 4-morpholinobenzaldehyde (1.1 eq), 160°C, 50 min followed by dilution with isopropanol to induce precipitation (78% yield); *c*, *N*-(2-(2-(2-aminoethoxy)ethoxy)ethyl)-5-(2-oxohexahydro-1*H*-thieno[3,4-*d*]imidazol-4-yl)pentanamide (2 eq), 1-ethyl-3-(3-dimethylaminopropyl)carbodiimide hydrochloride (2 eq), 1-hydroxybenzotriazole (2 eq), triethylamine (2 eq), 12 h, 25°C (37% yield).

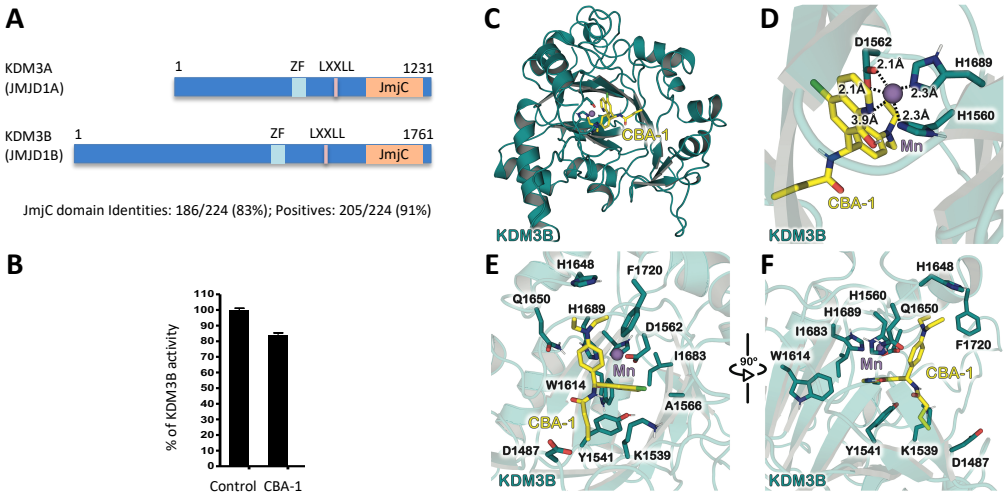

Figure S3. Molecular modeling of the binding site of KDM3B with CBA-1. **Related to Figure 4.**

A. The structures of KDM3A and KDM3B. **B.** Activity of **CBA-1** in KDM3B inhibition. **C.** Global view of the binding of **CBA-1** to KDM3B. Cartoon model representations are shown of the KDM3A in teal. **CBA-1** is shown in stick model and colored yellow. **D**. Local view of the Mn^{2+} binding site including **CBA-1**. Residues involved in the binding site are shown with stick model and colored the same color as its protein backbone. Dashed lines represent the coordination with distances shown close to the respective lines. **E**. Shown here is KDM3B with a focus on the side chain residue interactions between **CBA-1** and residues of KDM3B. **F**. Shown here is **CBA-1** surrounded by residues of KDM3B that are within 3 Å of the inhibitor.

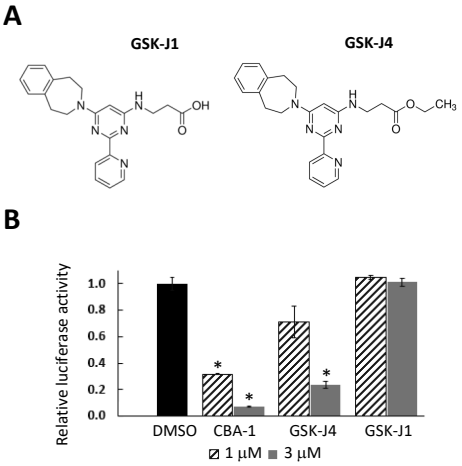

Figure S4. Structures and activities of GSK-J1 and GSKJ4. Related to Figure 4.

A. Structures of GSK-J1 and GSK-J4. **B**. Effects of GSK-J1 and GSK-J4 on Wnt signaling (* $p < 0.0001$; $n = 3$).

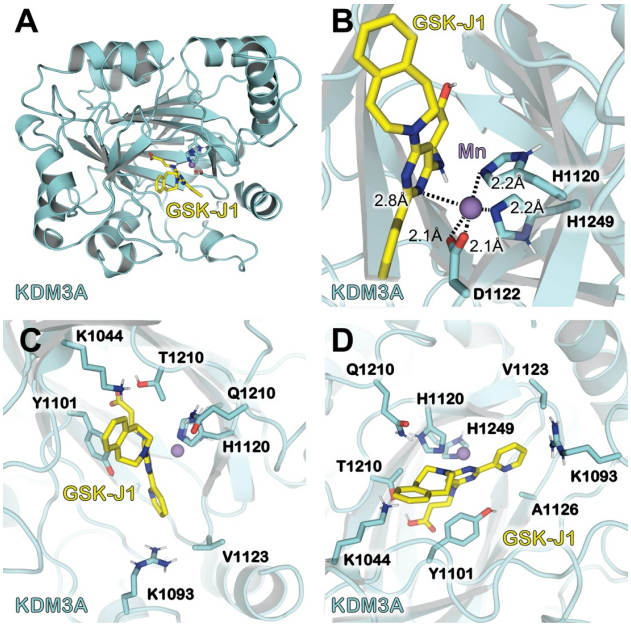

Figure S5. Molecular modeling of the binding site of KDM3A with GSK-J1. Related to Figure 4.

A. Global view of the binding of GSK-J1 to KDM3A. Cartoon representations are shown of the KDM3A in cyan. GSK-J1 is shown in stick model and colored yellow. **B**. Local view of the Mn^{2+} binding site including GSK-J1. Residues involved in the binding site are shown in stick model and colored the same color as its protein backbone. Dashed lines represent the coordination with distances shown. **C**. Shown here is GSK-J1 surrounded by residues of KDM3A that are within 4 Å of the inhibitor. **D**. Shown here is an alternative view of GSK-J1 and the surrounding KDM3A residues.

TRANSPARENT METHODS

Chemistry

Chemicals were purchased from either Millipore Sigma (St. Louis, MO) or Fisher Scientific (Hampton, NH) unless otherwise specified. Solvents were used from commercial vendors without further purification unless otherwise noted. Nuclear magnetic resonance spectra were acquired on a Varian (^{1}H at 400MHz; ^{13}C at 100MHz) instrument. High resolution electrospray ionization (ESI) mass spectra were recorded on an LTQ-Orbitrap Velos mass spectrometer (Thermo Fisher Scientific, Waltham, MA, USA). The FT resolution was set at 100,000 (at 400 *m*/*z*). Samples were introduced through direct infusion using a syringe pump with a flow rate of 5μL/min. Compounds were chromatographed on preparative layer Merck silica gel F254 (Fisher Scientific) plates unless otherwise indicated.

***N*-((5-Chloro-8-hydroxyquinolin-7-yl)(4-(diethylamino)phenyl)methyl)butyramide (CBA-1).** A mixture of 300 mg (1.67 mmol, 1 eq) of 5-chloroquinolin-8-ol, 300 mg (1.67 mmol, 1 eq) of 4-(diethylamino)benzaldehyde, and 580 mg (6.68 mmol, 4 eq) of butyramide was stirred at 130ºC for 2 h. The heating bath was removed, and 3 mL of isopropanol were added to the mixture. The mixture was allowed to cool 25ºC, and a precipitate was collected by filtration to provide 510 mg (71%) of **CBA-1**: mp 195-197°C. ^{1}H NMR (400 MHz, DMSO-d_6) δ 10.16 (s, 1H), 8.94 (dd, J = 4.2, 1.6 Hz, 1H), 8.59 (d, J = 8.6 Hz, 1H), 8.47 (dd, J = 8.5, 1.6 Hz, 1H), 7.73 (s, 1H), 7.7 (dd, J = 8.6, 4.2 Hz, 1H), 7 (d, J = 8.6 Hz, 2H), 6.57 (d, J = 8.7 Hz, 2H), 6.54 (d, J = 8.8 Hz, 1H), 3.27 (q, J = 7 Hz, 4H), 2.18 (t, J = 7.3 Hz, 2H), 1.64-1.45 (m, 2H), 1.03 (t, J = 7 Hz,

6H), 0.86 (t, *J* = 7.4 Hz, 3H). ^{13}C NMR (101 MHz, DMSO-d_6) δ 171.2, 149.05, 148.85, 146.33, 138.62, 132.45, 128.03 (two C), 127.95, 126.51, 126.21, 124.57, 122.71, 118.36, 111.32 (two C), 49.01, 43.61(two C), 37.25, 18.83, 13.63, 12.39 (two C). HRMS (ESI) Calcd for $C_{24}H_{29}ClN_3O_2$ [MH^+]: 426.1943. Found: 426.1946.

***N*-(2-(2-(2-(2-((7-(Butyramido(4-(diethylamino)phenyl)methyl)-5-chloroquinolin-8-yl)oxy)acetamido)ethoxy)ethoxy)ethyl)-5-((*3aR,4R,6aS*)-2-oxohexahydro-1*H*-thieno[3,4-*d*]imidazol-4-yl)pentanamide (CBA-B1)**. To a solution of 51 mg (0.12 mmol) of **CBA-1** in 0.5 mL of N,N-dimethylformamide (DMF) were added 22 mg (0.16 mmol, 1.3 eq) of potassium carbonate. The suspension was stirred for 15 min at 25ºC, and 50 mg (0.12 mmol, 1 eq) of *N*-(2-(2-(2-iodoethoxy)ethoxy)ethyl)-5-(2-oxohexahydro-1*H*-thieno[3,4-*d*]imidazol-4-yl)pentanamide was added. The mixture was stirred at 80ºC for 4 h. After cooling to room temperature, the mixture was poured into water, extracted with dichloromethane, dried over magnesium sulfate and concentrated. The crude product was purified by chromatography using 1:10 methanol-dichloromethane (R_f 0.33) to provide 21 mg (20%) of **CBA-B1**. ^{1}H NMR (400 MHz, $CDCl_3$-*d*) δ 8.95-8.86 (m, 1H), 8.6 (q, *J* = 13.2, 6.2 Hz, 1H), 8.54 (dd, *J* = 8.6, 1.7 Hz, 1H), 7.64 (d, *J* = 2.1 Hz, 1H), 7.52 (ddd, *J* = 8.5, 4.2, 1.4 Hz, 1H), 7.05 (d, *J* = 8.7 Hz, 2H), 6.58 (d, *J* = 8.8 Hz, 2H), 6.54 (d, *J* = 6.8 Hz, 1H), 6.45 (t, *J* = 6.4 Hz, 1H), 5.78 (s, 1H), 5.74 (s, 1H), 4.94 (d, *J* = 6.6 Hz, 1H), 4.82 (dd, *J* = 14.6, 5.9 Hz, 1H), 4.47-4.38 (m, 2H), 4.27-4.19 (m, 1H), 3.72-3.63 (m, 4H), 3.63-3.57 (m, 4H), 3.5 (t, *J* = 5.1 Hz, 2H), 3.4-3.26 (m, 6H), 3.14-3.03 (m, 1H), 2.86 (dd, *J* = 12.8 and 5 Hz, 1H), 2.67 (dd, *J* = 12.8, 4.4 Hz, 1H), 2.29-2.22 (m, 2H), 2.15-2.07 (m, 2H), 1.71-1.64 (m, 3H), 1.63-1.53 (m, 3H), 1.45-1.32 (m, 2H), 1.12 (t, *J* = 7 Hz, 6H), 0.96 (t, *J* = 7.4 Hz, 3H). ^{13}C NMR (101 MHz, $CDCl_3$) δ 173.26, 172.57, 169.82, 163.37, 150.6, 150.26, 147.58,

143, 135.31, 135.29, 133.61, 128.61, 126.93, 126.8, 126.18, 125.74, 122.18, 111.89, 77.36, 73.88, 70.44, 70.33, 70, 61.87, 60.19, 55.4, 52.29, 44.47, 40.64, 39.26, 39.12, 38.64, 35.83, 28.14, 25.56, 19.31, 13.99, 12.66. HRMS (ESI) Calcd for $C_{42}H_{59}ClN_7O_7S$ [MH^+]: 840.3880. Found: 840.3876.

1-(4-(Butyramido(5-chloro-8-hydroxyquinolin-7-yl)methyl)phenyl)-*N*-(2-(2-(2-(5-((*3aS,4S,6aR*)-2-oxohexahydro-1*H*-thieno[3,4-*d*]imidazol-4-yl)pentanamido)ethoxy)-ethoxy)ethyl)piperidine-4-carboxamide (CBA-B2). To a stirred solution of 120 mg (0.53 mmol) of 1-(4-formylphenyl)piperidine-4-carboxylic acid in 2 ml of DMF was added successively 100 mg (0.80 mmol, 1.5 eq) of 1-hydroxybenzotriazole (HOBt), 150 mg (0.8 mmol, 1.5 eq) of *N*-(3-dimethylaminopropyl)-*N'*-ethylcarbodiimide hydrochloride, 200 mg (0.53 mmol, 1 eq) of *N*-(2-(2-(2-aminoethoxy)ethoxy)ethyl)-5-(2-oxohexahydro-1*H*-thieno[3,4-*d*]imidazol-4-yl)pentanamide and 54 mg (0.8 mmol, 1.5 eq) of triethylamine. The mixture was stirred for 12 h at 25ºC, poured in brine, extracted with dichloromethane, dried over magnesium sulfate and concentrated. The crude product was purified by chromatography using 1:10 methanol-dichloromethane (R_f 0.18) to provide 180 mg (57%) of 1-(4-formylphenyl)-*N*-(2-(2-(2-(5-(2-oxohexahydro-1*H*-thieno[3,4-*d*]imidazol-4-yl)pentanamido)ethoxy)ethoxy)ethyl)-piperidine-4-carboxamide. A mixture of 110 mg (0.19 mmol) of this aforementioned carboxamide, 33 mg (0.19 mmol, 1 eq) of 5-chloroquinolin-8-ol, and 97 mg (1.12 mmol, 6 eq) of butyramide was stirred at 150ºC for 2 h. The heating bath was removed, and 2 mL of methanol were added to the mixture. The mixture was allowed to cool 25ºC, and a precipitate was collected by filtration. The precipitate was purified by chromatography using 1:10 methanol-dichloromethane (R_f 0.2) to provide 180 mg (57%) of **CBA-B2**. ^{1}H NMR (400 MHz, DMSO-d_6) δ 10.21 (s, 1H), 8.95 (d, *J* =

3.1 Hz, 1H), 8.64 (d, *J* = 8.7 Hz, 1H), 8.48 (d, *J* = 8.5 Hz, 1H), 7.83 (q, *J* = 6.1 Hz, 2H), 7.74-7.69 (m, 1H), 7.06 (d, *J* = 8.6 Hz, 2H), 6.86 (d, *J* = 8.5 Hz, 2H), 6.59 (d, *J* = 8.7 Hz, 1H), 6.4 (s, 1H), 6.34 (s, 1H), 4.38-4.23 (m, 1H), 4.17-4.06 (m, 1H), 3.65 (d, *J* = 12.3 Hz, 2H), 3.54-3.47 (m, 4H), 3.43-3.36 (m, 4H), 3.22-3.14 (m, 4H), 3.13-3.03 (m, 1H), 2.8 (dd, *J* = 12.4, 5 Hz, 1H), 2.66-2.53 (m, 3H), 2.31-2.21 (m, 1H), 2.18 (t, *J* = 7.3 Hz, 2H), 2.06 (t, *J* = 7.4 Hz, 2H), 1.78-1.38 (m, 11H), 1.34-1.2 (m, 2H), 0.86 (t, *J* = 7.4 Hz, 3H). ^{13}C NMR (101 MHz, DMSO-d_6) δ 174.31, 172.1, 171.27, 162.67, 150.01, 149.1, 148.95, 138.62, 132.47, 131.68, 127.66, 126.21, 126.13, 124.64, 122.79, 118.42, 115.64, 69.52, 69.14, 69.05, 61.02, 59.17, 55.4, 48.96, 48.38, 41.69, 38.42, 37.24, 35.09, 28.18, 28.02, 27.96, 25.25, 18.81, 13.61. HRMS (ESI) Calcd for $C_{42}H_{57}ClN_7O_7S$ [MH^+]: 838.3723. Found: 838.3730.

***N*^{1}-((5-Chloro-8-hydroxyquinolin-7-yl)(4-morpholinophenyl)methyl)-*N*^{4}-((2-(2-(5-((*3aS,4S,6aR*)-2-oxohexahydro-1*H*-thieno[3,4-*d*]imidazol-4-yl)pentanamido)-ethoxy)ethoxy)methyl)succinamide (CBA-B3).** A mixture of 300 mg (1.67 mmol) of 5-chloroquinolin-8-ol, 350 mg (1.84 mmol, 1.1 eq) of 4-morpholinobenzaldehyde, and 200 mg (1.67 mmol, 1 eq) of succinamic acid was stirred at 160ºC for 1 h. The heating bath was removed, and 3 mL of isopropanol were added to the mixture. The mixture was cooled to 25˚C, and a precipitate was collected by filtration to provide 380 mg (48%) of crude 4-(((5-chloro-8-hydroxyquinolin-7-yl)(4-morpholinophenyl)methyl)amino)-4-oxobutanoic acid. To a stirred solution of 63 mg (0.13 mmol) of this crude product in 1 mL of DMF were successively added 36 mg (0.27 mmol, 2 eq) of 1-hydroxybenzotriazole (HOBt), 51 mg (0.27 mmol, 2 eq) of *N*-(3-dimethylaminopropyl)-*N*′-ethylcarbodiimide hydrochloride, 50 mg (0.13 mmol, 1 eq) of *N*-(2-(2-(2-aminoethoxy)ethoxy)ethyl)-5-(2-oxohexahydro-1*H*-thieno[3,4-*d*]imidazol-4-yl)pentanamide

and 37 mL (0.27 mmol, 2 eq) of triethylamine. The mixture was stirred for 12 h at 25ºC and poured into water. A precipitate was collected by filtration to provide 41 mg (37%) of pure **CBA-B3**. ^{1}H NMR (400 MHz, DMSO-d_6) δ 10.19 (s, 1H), 8.91 (dd, J = 4.2, 1.6 Hz, 1H), 8.68 (d, J = 8.7 Hz, 1H), 8.44 (dd, J = 8.6, 1.6 Hz, 1H), 7.84 (t, J = 5.6 Hz, 1H), 7.79 (t, J = 5.7 Hz, 1H), 7.7-7.63 (m, 1H), 7.07 (d, J = 8.7 Hz, 2H), 6.83 (d, J = 8.8 Hz, 2H), 6.56 (d, J = 8.7 Hz, 1H), 6.37 (s, 1H), 6.31 (s, 1H), 4.31-4.22 (m, 1H), 4.15-4.04 (m, 1H), 3.69-3.63 (m, 4H), 3.44 (s, 4H), 3.38-3.31 (m, 4H), 3.14 (q, J = 5.9 Hz, 4H), 3.08-3.03 (m, 2H), 3.03-2.98 (m, 4H), 2.77 (dd, J = 12.4, 5.1 Hz, 1H), 2.53 (d, J = 12.5 Hz, 1H), 2.44-2.38 (m, 2H), 2.31 (d, J = 6.9 Hz, 2H), 2.02 (t, J = 7.4 Hz, 2H), 1.63-1.5 (m, 1H), 1.51-1.35 (m, 3H), 1.32-1.18 (m, 2H). ^{13}C NMR (101 MHz, DMSO-d_6) δ 172.12, 171.37, 170.65, 162.68, 150.01, 149.1, 148.89, 138.62, 132.48, 127.6, 126.24, 126.06, 124.68, 122.81, 118.52, 115.02, 69.5, 69.15, 69.09, 66.04, 61.02, 59.18, 55.41, 48.96, 48.55, 39.83, 38.54, 38.43, 35.09, 30.76, 30.67, 28.18, 28.03, 25.25. HRMS (ESI) Calcd for $C_{40}H_{53}ClN_7O_8S$ [MH^+]: 826.3359. Found: 826.3357.

Biology

Drug screening. Stable HEK293T cell line transfected with a TOPFlash plasmid was treated with DMSO or 2.5 μM of each compound. After 6 h, the cells were treated with 25 mM LiCl to activate Wnt signaling. The inhibition ratios of these compounds were determined. The leading compounds were validated at 500 nM. The compound library was from University of Cincinnati Drug Discovery Center.

Cell culture. LS174T colon cancer cells were cultured in EMEM (ATCC, 30-2003) containing 10% Fetal Bovine Serum (Sigma F0926). HEK293T and the DLD-1 and SW620 colon cancer cells were cultured in DMEM (Sigma D6429) containing 10% Fetal Bovine Serum (Sigma, F0926). For proliferation assays, cells ($3.5x10^4$ cells per well) were split into 12-well plates. After 24 h, 1 μl of each compound was added to each well. DMSO was used as a control. Each experiment was done in triplicate. Cell viability and number were analyzed using the Vi-Cell XR Cell Viability Analyzer (Beckman Coulter). ShRNA construct for KDM3A was ordered from Sigma. HEK293T cells were transfected with lentivirus packaging plasmids psPAX2 and pMD2.G, as well as control shRNA plasmids. Lentivirus stock was collected 48h after transfection. Cells were infected by the lentivirus stock for 12h, followed by sustained growth in fresh medium for 36-48h. Infected cell lines were seeded in 12-well plate for proliferation assay. ShRNA efficiency was tested by Western blotting using lysates from HEK293T or colon cancer cells transfected with shRNAs. Wnt reporter assay has been described previously(Shi et al., 2015, Zhang et al., 2019).

Biochemistry. Western blotting: Cells were lysed in the appropriate volume of lysis buffer (50 mM HEPES, 100 mM NaCl, 2 mM EDTA, 1% glycerol, 50 mM NaF, 1 mM Na_3VO_4, 1% Triton X-100, with protease inhibitors). KDM3A and KDM3B inhibition assays were performed through the service of BPS Bioscience (San Diego, CA). Antibodies for Wnt target genes, such as Axin2, c-Myc, survivin, cyclin B1 and cyclin D1 have been described previously(Shi et al., 2015, Zhang et al., 2011). KDM3A antibody was purchased from GeneTex (GTX129046). Histone methylation antibodies were purchased from Cell Signaling Technology. To validate the **CBA-1** target, HEK293T cell lysates were incubated with streptavidin beads and biotinylated

CBA-B2 at 4ºC overnight. The beads were washed 3 times with cell lysis buffer and the binding proteins were analyzed by Western blot as previously described(Zhang et al., 2013). Chromatin immunoprecipitation (ChIP) assay was performed with Di-Methyl-Histone H3 (Lys9) antibody (#4658) from Cell Signaling Technology using the method previously described(Evans et al., 2007). The Western blot images were scanned using CanoScan 5600F and the densitometry was analyzed using Adobe photoshop 2020. Real-time qPCR was perform using QuantStudio 3 from Applied Biosystems.

Colon Cancer Organoids. The colon cancer organoids were provided by Professor Tianyan Gao at Markey Cancer Center, University of Kentucky. The organoids were isolated from $Apc^{f/+}$/$Kras^{LSL\text{-}G12D}$/Villin-Cre mouse model(Wen et al., 2017). For 48-well drug screening, the Matrigel containing organoids was digested by 300 µl dispase. The gel was removed by 1000 x 5min spinning. The organoids were digested into single cells by 1 ml Trypsin and washed with 10 ml Advanced DMEM/F12. For each well, 80 µl Matrigel was added to the bottom and 500 cells in 60 µl Matrigel were added to the top. The cells were culture in 250 µl 3D complete medium (Advanced DMEM/F12 supplemented with 1 x N-2, 1 x B-27, 1 mmol/l N-acetylcysteine and 1% penicillin/streptomycin). The cells were treated with DMSO or testing compounds and organoids formation were analyzed using microscope.

Zebrafish Studies. Use and handling of Zebrafish was approved by the University of Kentucky's Institutional Animal Care and Use Committee (IACUC), protocol 2015-2225. For eye phenotype studies, CG1 syngeneic Zebrafish were dechorionated using 1 mg/mL Pronase and treated at 6 hours post-fertilization (hpf) with DMSO, or 1 µM Bio (Millipore Sigma,

B1686-5MG) with or without varying concentrations of **CBA-1** in 200 µL E3 media in 96-well plates. Eye development was assessed after 2 days of treatment. 6xTCF/LEF-miniP:eGFP sheer transgenic Zebrafish (a kind gift from Dave Langenau, Harvard University, Boston, MA) were utilized to assess Wnt signaling *in vivo*. Zebrafish were dechorionated as above at 24 hpf and treated with DMSO, Bio, or **CBA-1** in a 96-well plate in 200 µL E3 media volume. Zebrafish were imaged after 48 hours of treatment. For tail amputation studies, adult 6xTCF/LEF-miniP:eGFP sheer transgenic Zebrafish were anesthetized with Tricaine (Pentair, TRS1) and a single cut was made with a razor blade perpendicular to the fin rays. Fish were allowed to recover for 20 minutes before randomly dividing the fish into treatment groups. Fish were kept in DMSO, 1 µM Bio, or 5 µM **CBA-1** in 250 mL of fish system water for 5 days post-amputation. Drug was changed daily, and the fish were fed on day 2 post-amputation prior to drug change. Fish were imaged and tail growth was assessed at 4 days post-amputation.

Molecular Modeling. Molecular modeling was conducted to determine the KDM3A structure using the KDM3B structure as a template. The KDM3B structure was obtained from a 2.18 Å X-ray crystal structure with RCSB Protein Data Bank (PDB) ID 4C8D. Modeller(Webb and Sali, 2016) was used to build the KDM3A structure and add missing residues to the protein. The homology modeled structure of KDM3A was then energy minimized with 4,000 steps of the deepest decent energy-minimization and 4,000 steps of the conjugate gradient energy-minimization by using the Sander module of the Amber18 package(Case et al., 2018).

Molecular Docking. Molecular docking was conducted to determine the binding poses of inhibitors **CBA-1** and GSK-J1 within the JmjC domain of KDM3A or KDM3B. Gold docking

program(Verdonk et al., 2004, Verdonk et al., 2003) was used to carry out the docking at the metal ion binding site. All structures were imported into the LEaP module of the Amber18(Case et al., 2018) suite of programs(Case et al., 2005) to add hydrogens using the ff14SB(Hornak et al., 2006, Maier et al., 2015) modified version of the Cornell et al.(Cornell et al., 1995) force field. These structures were optimized with 4,000 steps of the deepest decent energy-minimization and 4,000 steps of the conjugate gradient energy-minimization by using the Sander module of the Amber18 package. This series of optimized minimization steps were carried out by applying a harmonic constraint only on the protein and gradually reducing the force constant from 300, 200, 100, 75, 50, and 25 kcal/mol/Å^2. A final minimization step was carried out without applying any harmonic constraint. The figures showing the structures were generated using the PyMol software.(Schrodinger, 2015)

Statistics. Cell proliferation, Western blot, report assay and real-time PCR were performed in triplicates. Microarray and patient clinical data from colon cancer studies were downloaded from the TCGA and GTEx databases. A two-sample t-test was used to compare KDM3A expression in colon adenocarcinoma patients versus normal controls using GEPIA program.[25]

Table S1. Key Resources. Related to all Figures.

REAGENT or RESOURCE	SOURCE	IDENTIFIER
Antibodies		
Rabbit monoclonal anti-c-Myc (N-term)	Abcam	Cat# 1472-1, RRID:AB_562270
Rabbit monoclonal anti-Axin2 (76G6)	Cell Signaling Technology	Cat# 2151, RRID:AB_2062432
Rabbit monoclonal anti-Cyclin d1	Abcam	Cat# 2261-1, RRID:AB_991714
Mouse monoclonal anti-Cyclin B1 (V152)	Cell Signaling Technology	Cat# 4135, RRID:AB_2233956
Rabbit monoclonal anti-Survivin (71G4B7)	Cell Signaling Technology	Cat# 2808, RRID:AB_2063948
Mouse monoclonal anti-beta-Actin	Sigma-Aldrich	Cat# A1978, RRID:AB_476692
Rabbit monoclonal anti-Tri-Methyl-Histone H3 (Lys9) (D4W1U)	Cell Signaling Technology	Cat# 13969, RRID:AB_2798355
Rabbit monoclonal anti-Di-Methyl-Histone H3 (Lys9) (D85B4)	Cell Signaling Technology	Cat# 4658, RRID:AB_10544405
Rabbit monoclonal anti-Di-Methyl-Histone H3 (Lys4) (C64G9)	Cell Signaling Technology	Cat# 9725, RRID:AB_10205451
Rabbit polyclonal anti-Histone H3	Abcam	Cat# ab1791, RRID:AB_302613
Mouse monoclonal anti-GAPDH (GT239)	GeneTex	Cat# GTX627408, RRID:AB_11174761
Rabbit polyclonal anti-KDM3A	GeneTex	Cat# GTX129046
Goat Anti-Rabbit IgG, H & L Chain Specific Peroxidase Conjugate	Millipore	Cat# 401315, RRID:AB_2617117
Goat Anti-Mouse IgG, H & L Chain Specific Peroxidase Conjugate	Millipore	Cat# 401215, RRID:AB_10682749
Bacterial and Virus Strains		
N/A		
Biological Samples		
N/A		
Chemicals, Peptides, and Recombinant Proteins		
XAV939	Sigma-Aldrich	Cat# X3004-5MG; CAS: 284028-89-3
LiCl	Sigma-Aldrich	Cat# L4408-100G; CAS: 7447-41-8
Dimethyl sulfoxide	Sigma-Aldrich	Cat# D2650-100ML; CAS: 67-68-5
Strep-Tactin Superflow Agarose	Millipore	Cat# 71592-3
BIO	Sigma-Aldrich	Cat# B1686; CAS: 667463-62-9
GSK-J1 (sodium salt)	Cayman Chemical	Cat# 12054; CAS: 1797832-71-3
GSK-J4 (hydrochloride)	Cayman Chemical	Cat# 12073; CAS: 1797983-09-5
Critical Commercial Assays		
Dual-Luciferase Reporter Assay System	Promega	Cat# 1910
Vi-Cell XR Reagent Pack for Cell viability analyzer	BECKMAN	Cat# 383260
JMJD1A Homogeneous Assay Kit	BPS Bioscience	Cat# 50412

Deposited Data		
N/A		
Experimental Models: Cell Lines		
Human: 293T Cells	ATCC	Cat# CRL-3216; RRID:CVCL_0063
Human: LS174T Cells	ATCC	Cat# CL-188; RRID:CVCL_1384
Human: SW620 Cells	ATCC	Cat# CCL-227; RRID:CVCL_0547
Human: DLD-1 Cells	ATCC	Cat# CCL-221; RRID:CVCL_0248
Mouse: L Wnt-3A Cells	ATCC	Cat# CRL-2647; RRID:CVCL_0635
Experimental Models: Organisms/Strains		
6xTCF/LEF-miniP:eGFP sheer transgenic Zebrafish	Kind gift from Dave Langenau at Harvard University	N/A
Mouse colon cancer organoids from $Apc^{f/+}/Kras^{LSL-G12D}$/Villin-Cre mouse model	Kind gift from Tianyan Gao at University of Kentucky	N/A
Oligonucleotides		
C-Myc ChIP Primers: Forward: GTGAATACACGTTTGCGGGTTAC; Reverse: AGAGACCCTTGTGAAAAAAACCG	This paper	N/A
Cyclin B1 ChIP primers: Forward: TCTTGCCCGGCTAACCTTTCCAGG; Reverse: TTCCGCCGCAGCACGCCGAGAAGA	This paper	N/A
GAPDH ChIP primers: Forward: CATGTTCGTCATGGGGTGAACCA; Reverse: AGTGATGGCATGGACTGTGGTCAT	This paper	N/A
Recombinant DNA		
pLKO human KDM3A shRNA	Sigma-Aldrich	TRCN0000329990
Software and Algorithms		
Graphpad Prism 5	Graphpad	RRID:SCR_002798 http://www.graphpad.com
GEPIA	Peking University	RRID:SCR_018294 http://gepia.cancer-pku.cn
GOLD	CCDC	RRID:SCR_000188 http:/www.ccdc.cam.ac.uk/Solutions/GoldSuite/Pages/GOLD.aspx
MODELLER	Ben Webb	RRID:SCR_008395 http://salilab.org/modeller/modeller.html
Other		

SUPPLEMENTAL REFERENCES

CASE, D. A., BEN-SHALOM, I. Y., BROZELL, S. R., CERUTTI, D. S., CHEATHAM III, T. E., CRUZEIRO, V. W. D., DARDEN, T. A., DUKE, R. E., GHOREISHI, D., GILSON, M. K., GOHLKE, H., GOETZ, A. W., GREENE, D., HARRIS, R., HOMEYER, N., IZADI, S., KOVALENKO, A., KURTZMAN, T., LEE, T. S., LEGRAND, S., LI, P., LIN, C., LIU, J., LUCHKO, T., LUO, R., MERMELSTEIN, D. J., MERZ, K. M., MIAO, Y., MONARD, G., NGUYEN, C., NGUYEN, H., OMELYAN, I., ONUFRIEV, A., PAN, F., QI, R., ROE, D. R., ROITBERG, A., SAGUI, C., SCHOTT-VERDUGO, S., SHEN, J., SIMMERLING, C. L., SMITH, J., SALOMON-FERRER, R., SWAILS, J., WALKER, R. C., WANG, J., WEI, H., WOLF, R. M., WU, X., XIAO, L., YORK, D. M. & KOLLMAN, P. A. 2018. *AMBER 2018,* University of California, San Francisco.

CASE, D. A., CHEATHAM, T. E., DARDEN, T., GOHLKE, H., LUO, R., MERZ, K. M., ONUFRIEV, A., SIMMERLING, C., WANG, B. & WOODS, R. J. 2005. The Amber biomolecular simulation programs. *Journal of Computational Chemistry,* 26**,** 1668-1688.

CORNELL, W. D., CIEPLAK, P., BAYLY, C. I., GOULD, I. R., MERZ, K. M., FERGUSON, D. M., SPELLMEYER, D. C., FOX, T., CALDWELL, J. W. & KOLLMAN, P. A. 1995. A 2ND GENERATION FORCE-FIELD FOR THE SIMULATION OF PROTEINS, NUCLEIC-ACIDS, AND ORGANIC-MOLECULES. *Journal of the American Chemical Society,* 117**,** 5179-5197.

EVANS, P. M., ZHANG, W., CHEN, X., YANG, J., BHAKAT, K. K. & LIU, C. 2007. Kruppel-like factor 4 is acetylated by p300 and regulates gene transcription via modulation of histone acetylation. *J Biol Chem,* 282**,** 33994-4002.

HORNAK, V., ABEL, R., OKUR, A., STROCKBINE, B., ROITBERG, A. & SIMMERLING, C. 2006. Comparison of multiple amber force fields and development of improved protein backbone parameters. *Proteins-Structure Function and Bioinformatics,* 65**,** 712-725.

MAIER, J. A., MARTINEZ, C., KASAVAJHALA, K., WICKSTROM, L., HAUSER, K. E. & SIMMERLING, C. 2015. ff14SB: Improving the Accuracy of Protein Side Chain and Backbone Parameters from ff99SB. *Journal of Chemical Theory and Computation,* 11**,** 3696-3713.

SCHRODINGER, L. 2015. The PyMOL Molecular Graphics System, Version 1.8.

SHI, J., LIU, Y., XU, X., ZHANG, W., YU, T., JIA, J. & LIU, C. 2015. Deubiquitinase USP47/UBP64E Regulates beta-Catenin Ubiquitination and Degradation and Plays a Positive Role in Wnt Signaling. *Mol Cell Biol,* 35**,** 3301-11.

VERDONK, M. L., BERDINI, V., HARTSHORN, M. J., MOOIJ, W. T. M., MURRAY, C. W., TAYLOR, R. D. & WATSON, P. 2004. Virtual Screening Using Protein−Ligand Docking: Avoiding Artificial Enrichment. *Journal of Chemical Information and Computer Sciences,* 44**,** 793-806.

VERDONK, M. L., COLE, J. C., HARTSHORN, M. J., MURRAY, C. W. & TAYLOR, R. D. 2003. Improved protein–ligand docking using GOLD. *Proteins: Structure, Function, and Bioinformatics,* 52**,** 609-623.

WEBB, B. & SALI, A. 2016. Comparative Protein Structure Modeling Using MODELLER. *Curr Protoc Bioinformatics,* 54**,** 5.6.1-5.6.37.

WEN, Y. A., XING, X., HARRIS, J. W., ZAYTSEVA, Y. Y., MITOV, M. I., NAPIER, D. L., WEISS, H. L., MARK EVERS, B. & GAO, T. 2017. Adipocytes activate mitochondrial fatty acid oxidation and autophagy to promote tumor growth in colon cancer. *Cell Death Dis,* 8**,** e2593.

ZHANG, W., SVIRIPA, V., CHEN, X., SHI, J., YU, T., HAMZA, A., WARD, N. D., KRIL, L. M., VANDER KOOI, C. W., ZHAN, C. G., EVERS, B. M., WATT, D. S. & LIU, C. 2013. Fluorinated N,N-dialkylaminostilbenes repress colon cancer by targeting methionine S-adenosyltransferase 2A. *ACS Chem Biol,* 8**,** 796-803.

ZHANG, W., SVIRIPA, V., KRIL, L. M., CHEN, X., YU, T., SHI, J., RYCHAHOU, P., EVERS, B. M., WATT, D. S. & LIU, C. 2011. Fluorinated N,N-dialkylaminostilbenes for Wnt pathway inhibition and colon cancer repression. *J Med Chem,* 54**,** 1288-97.

ZHANG, W., SVIRIPA, V. M., KRIL, L. M., YU, T., XIE, Y., HUBBARD, W. B., SULLIVAN, P. G., CHEN, X., ZHAN, C. G., YANG-HARTWICH, Y., EVERS, B. M., SPEAR, B. T., GEDALY, R., WATT, D. S. & LIU, C. 2019. An Underlying Mechanism of Dual Wnt Inhibition and AMPK Activation: Mitochondrial Uncouplers Masquerading as Wnt Inhibitors. *J Med Chem,* 62**,** 11348-11358.